USE OF A STANTON THERMOBALANCE FOR MICROANALYSIS OF CREOSOTE

T. W. Smeal

United States Steel Corporation
Applied Research Laboratory
Monroeville, Pa.

Introduction

In the production of metallurgical coke by modern processes, the gases and tars driven from the coal are condensed to provide the raw material for a wide variety of coal chemicals. These coal chemicals, including millions of gallons of coal-tar creosote, are some of the important products of the United States Steel Corporation. As a major producer of coal-tar creosote, the Corporation has sought to learn more about the properties of creosote as a wood preservative.

One of the best methods for studying the chemistry of creosote as a wood preservative is to extract the residual creosote from wood that has been in service and for which a completely documented history is available. For analytical purposes, however, the amount of creosote that can be extracted from small core borings, sections of small test stakes, and other small specimens is not sufficient. Therefore the Applied Research Laboratory of the United States Steel Corporation initiated a search for a relatively simple method of characterizing very small samples (0.1 - 1.0 gram) to replace the Church-flask distillation, which requires a sample of 100 grams. The Church-flask distillation, which is accepted as the standard method for characterizing the composition of creosote, is fundamentally an evaporation method. Other apparatus that gives refined measurements of evaporation has been proposed by researchers at Allied Chemical Corporation and at Bell Telephone Laboratories.[1,2]* These methods, however, were not well-adapted to our problem. It was logical to reason that since we were interested in the evaporation pattern of a small amount of volatile materials, a controlled-temperature recording balance would reveal the desired pattern. Such an instrument was available in the form of a thermobalance manufactured by the Stanton Instrument Company of London.

The Stanton Thermobalance

The Stanton thermobalance, Model TR-1 shown in Figure 1, is an analytical, continuously recording balance so constructed that the sample being weighed is supported within a tube furnace. The electrically heated furnace is constructed to operate throughout a range of 1000 centigrade degrees. The temperature is automatically raised during the weighing period by means of a program control motor. Although motors of different speeds are obtainable, the work reported here was done with a motor providing a constant rate of six degrees per minute temperature rise. The tube furnace, which contains baffles to reduce air movement, is two inches in diameter and has a hot zone two inches in depth. A platinum-rhodium thermocouple located near the furnace wall at the center of the hot zone actuates the temperature-recording pen. The furnace can be easily raised and lowered over the sample on the balance platform. The sample, itself, is contained in a small crucible supported on a rod attached to the weighing mechanism of the balance. A system of guide rods and counterweight keeps the furnace symmetrically aligned with the axis of the crucible.

---

* See References.

The balance mechanism is sensitive to one milligram and can record a weight change as great as 400 milligrams per minute to a maximum total weight change of 50 grams.

Use of the Thermobalance

Because the temperature-recorder thermocouple is located along the wall of the furnace rather than in the crucible, a crucible of high heat-conductivity must be used to minimize the unavoidable lag in temperature of the sample. We used a 10 cc platinum crucible conforming to Standard D-271 of the American Society for Testing Materials. Experimentation with various covers on the crucible revealed that the best correlation with existing standard was obtained when the crucible was used without a cover.

The Church-flask method of distillation that has been adopted as the standard method for creosote characterization by the American Wood-Preservers' Association (AWPA)[3] and the American Society for Testing Materials (ASTM)[4] is basically a vaporization method because there is no attempt at rectifying the vapors. The major difference in the results obtained by these two methods is caused by the difference in methods of measuring the temperature and weighing the distillate. The Church-flask method measures the temperature at a point slightly above the liquid surface, but the distillate is not weighed until it has been collected in a flask at the end of a side-arm condenser, a distance of 52 to 55 centimeters. The weight of the distillate collected at the end of the condenser is, therefore, considerably less than the weight loss of the sample. The discrepancy is the amount of vapor and condensate held up in the flask and in the condenser. The discrepancy is particularly great during the early portion of the distillation. The thermobalance, however, weighs the residue the instant the vapor leaves the surface of the sample in the crucible. The vapor loss, which is the difference in weight between the weight of the original sample and the weight of the residue, is plotted against a continuous record of temperature. The thermobalance results are not retarded and correspond more nearly to a true measure of evaporation. Plateaus or flats that are observed in the distillation pattern obtained by high-reflux distillation are not recorded by the thermobalance because there is no rectification of vapors, and the temperature is driven upward at a constant rate.

Experience has shown that for reliable results the sensitive thermobalance should be placed on an island site, preferably on a concrete floor, away from heat of direct sunlight, dampness, drafts and changes in temperature. There was also an indication that barometric pressure affected the results. Although this influence was not evaluated, it was believed that any adjustment of results would be insignificant relative to the interpretation of the data.

Developing the Procedure

The first step in developing a procedure was to determine the reproducibility of results with the thermobalance. To do this, seven vaporization patterns were made using replicate 0.5 gram samples of one creosote (Figure 2). The range of values show an acceptable level of reproducibility. Vaporization patterns made during any one day agreed more closely than replicate runs made on successive days. We believe that changes in barometric pressure, ambient temperature, and localized drafts account for a large part of the variation encountered.

The next step was to correlate the results obtained by use of the thermobalance with patterns obtained by use of a Church flask and by use of a Snyder 5-ball distillation column. Distillation through a five-ball column was chosen because it is rapid and because it is used by some researchers in the field of wood preservation. The Church-flask method is the accepted standard of the American Wood-Preservers' Association. The similarities and differences between the results of these methods are shown in Figure 3. The thermobalance results are observed to

fall between those of the other two methods. The data show that the differences between the results of the Church-flask method and thermobalance method are due primarily to the lag observed in the use of the Church-flask. Differences between the results of the five-ball column and thermobalance methods are attributed to the rapid rate of temperature rise (6 C per minute), which does not permit enough time for the low-boiling materials within the liquid to diffuse to the surface. It appears that the differences all occur below about 300 C, and all three methods agree reasonably well above this point.

The final step was to determine the ability of the thermobalance to detect differences in creosote composition. This was done by preparing thermobalance vaporization patterns of a fresh creosote and distillation residues from the same creosote after distillates to temperatures of 210, 235, 270, and 315 C had been removed with a five-ball column (Figure 4). This figure clearly shows the effects of removing the low-boiling fractions of creosote. It was reasonable to expect that the effects of any process changing the composition of the creosote could be determined by comparing vaporization patterns. Therefore, the thermobalance vaporization pattern of the chemically changed creosote was superimposed on a similar figure made with a sample of the original creosote. In addition, the thermobalance vaporization pattern provided more information than the Church or five-ball column distillation methods because a higher temperature was obtained with the thermobalance.

Application of the Method

To test the method on actual extracts from creosoted wood, a number of 3/4- by 3/4- by 30-inch stakes were withdrawn from field exposure plots. These stakes had been impregnated with a variety of creosotes and then exposed outdoors for periods of five and ten years, respectively. Each stake was sawn in sections as shown in Figure 5 so that indications of changes in the composition of creosote relative to its position within the stake could be obtained. These sections were shaved individually into fine chips. The residual creosote in each lot of chips was extracted with aromatic solvents. The solvents were then stripped from each extract by distillation under reduced pressure.

These samples of residual creosote were characterized by vaporization on the thermobalance, and the results were graphed. To interpret these graphs, the vaporization patterns were compared with patterns of the original creosotes and with patterns of creosote residues boiling above selected temperatures.

The thermobalance vaporization patterns for the residual creosotes, Figures 6 and 7, from a stake that had been in field test for ten years show that considerable losses of the more volatile compounds have occurred from all sections of the stake. It is noteworthy that the vaporization patterns for all sections fall closely to the vaporization curve obtained from creosote residue boiling above 315 C. The similarity among these curves indicates that much of the creosote boiling up to 315 C has been lost. This loss is known to occur by means of evaporation and migration. If the loss were solely by unhindered evaporation, the curves of the extract and of the control should be very close to each other. If downward migration of residual creosote occurs, then a concentration of high-boiling material can be expected in the lower portion of the stake. Such migration can be expected to appear as a net gain in preservative concentration at the lower end of the stake. This concentration was actually observed. Both below-ground sections retained about 0.08 gram of residual creosote per cubic centimeter of wood. The two sections above ground contained less than 0.05 gram per cubic centimeter.

Figure 6 shows, however, that there is considerable disparity between the vaporization curves of extracts from Section 1 and Section 2, both taken from below the groundline. What then can account for the apparent differences in composition of these extracts? We believe that soon after driving the test stake into the ground, some of the creosote begins to migrate downward through the porous cellular structure

of the wood. As it moves downward, a portion of the low-boiling volatile components are lost by evaporation from the surface of the stake. When the moving creosote approaches the moist groundline section, the downward migration is counteracted by the upward movement of moisture from the soil through the wick-like behavior of the stake. In the section of the stake just below the groundline, the net effect of these counter movements is such as to cause a concentration of creosote. This creosote by now is partially depleted of low-boiling volatile components, and has a high proportion of high-boiling relatively stable components. This concentration of high-boiling material is indicated by the relatively low position of the right end of the vaporization curve for the extract from Section 2.

If we convert the percentages of material boiling above 380 C to absolute amounts of that fraction remaining in the wood, it is found that the quantity of this fraction in Sections 3 and 4 is the same as was impregnated into the wood originally. Below ground, in Sections 1 and 2, the amount of this high-boiling fraction was about twice as great as in the freshly impregnated stake. This increase can result only from chemical changes in the creosote itself. These chemical changes are believed to result primarily from oxidation and polymerization reactions.

Figure 8 shows similar vaporization patterns for Sections 1 and 2 of a stake that had been in field test for only five years. These vaporization patterns lie between the control patterns for residues boiling above 235 and 270 C. Comparison with Figure 6 indicates that evaporation of the creosote has not progressed to the extent observed in the 10-year-old stake. Because the vaporization curves closely parallel the control curves, the chemical change is believed to be relatively small.

Summary

1. The Stanton Thermobalance can quickly and effectively characterize small (0.1 to 1.0 gram) samples of creosote.

2. The continuous vaporization pattern produced by the thermobalance is similar to that of both the Church-flask distillation (adopted by the AWPA and ASTM) and distillation through a five-ball column. The record of weight loss resulting from vaporization on the thermobalance is not retarded, as it is in a Church distillation, and thus is closer to a true measure of evaporation.

3. A method has been developed for estimating the extent of losses of creosote through evaporation.

4. A method has been developed for estimating the relative extent of chemical modifications that have occurred in wood in service during weathering.

5. Natural factors that are conducive to chemical modification of creosote appear to have their greatest effect at the ground line.

References

1. Stasse, H. L., "A Simple Fractional Distillation Test for Creosote," Proceedings, American Society for Testing Materials, 1954.

2. Leutritz, John, Jr., W. McMahon, and G. D. Deeg, "Relationship of Evaporation Pattern and Distillation Characteristics of Coal Tar Creosote," Proceedings, American Wood-Preservers' Association, 1959.

3. American Wood-Preservers' Association "Manual of Recommended Practice," Section A1-58, p 3.

4. American Society for Testing Materials "Standards," Part 4, pp 751-756 (1949).

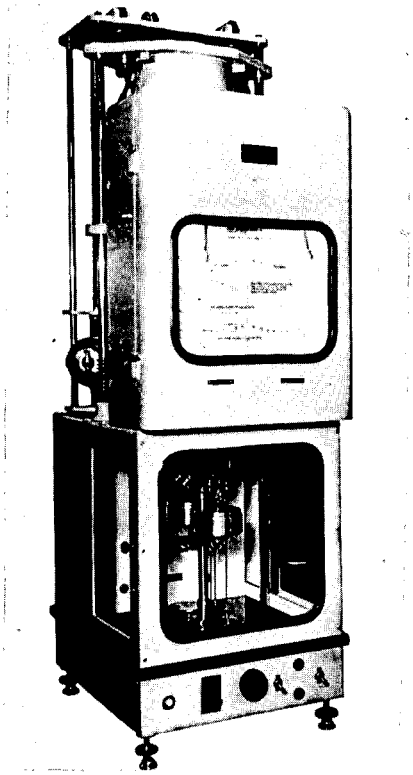

Figure 1. The Stanton Thermobalance.

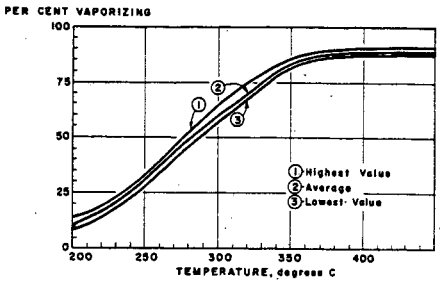

Figure 2. Range of Results From Seven Replicate Runs in Thermobalance.

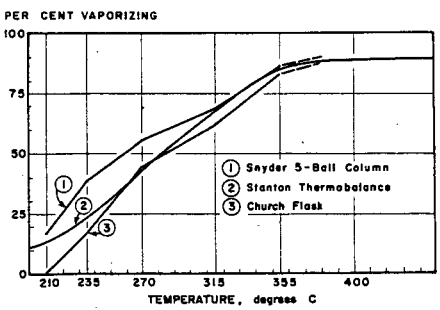

Figure 3. Characteristics of a Creosote Analyzed by Three Different Methods.

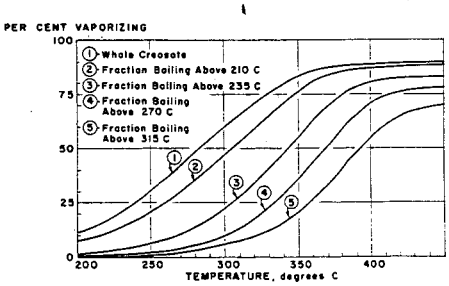

Figure 4. Vaporization Patterns From Whole Creosote and Four of Its Distillation Fractions.

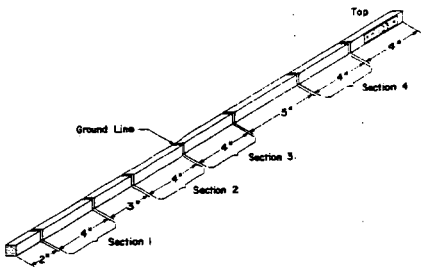

Figure 5. Position of Sections Cut From 3/4-Inch Square Stake for Extraction of Residual Creosote.

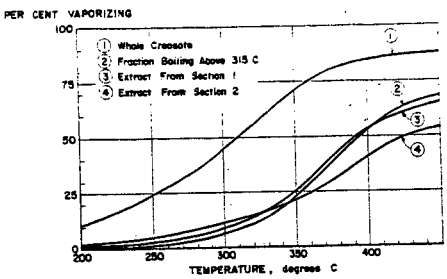

Figure 6. Changes in Creosote Resulting From Ten Years Exposure in Wood Below Ground.

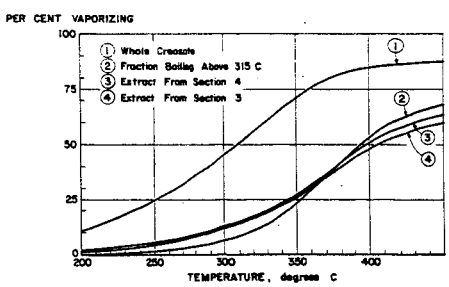

Figure 7. Changes in Creosote Resulting From Ten Years Exposure in Wood Above Ground.

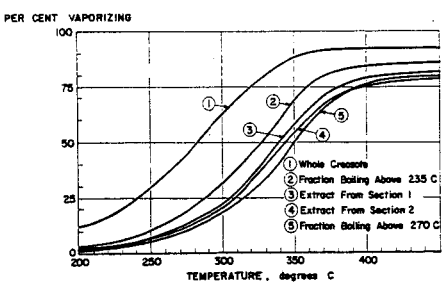

Figure 8. Changes in Creosote Resulting From Five Years Exposure in Wood Below Ground.

A RE-INVESTIGATION OF DENSIMETRIC METHODS OF RING ANALYSIS

Teh Fu Yen, J. Gordon Erdman, and William E. Hanson

Mellon Institute
Pittsburgh 13, Pennsylvania

For many years the chemist has sought a method whereby the average structural character of the molecules in a complex mixture might be determined. In general, two types of mixtures have received most attention. One has consisted of mixtures of compounds comprising a relatively narrow molecular weight range and where the average molecular weight could be obtained; examples are narrow boiling cuts from petroleum. The second has consisted of very complex systems, such as coals, where molecular weight could not be determined, and, indeed, where the concept of molecular weight might not be applicable.

Present studies in this laboratory have as their objective clarification of the structure of the asphaltic, non-hydrocarbon constituents of crude oil and of the presumably similar, but higher molecular weight, black, insoluble organic fraction of ancient sedimentary rocks. From the point of view of structural type analysis, these substances represent a situation somewhere between that of a low molecular weight hydrocarbon mixture and the macromolecular structure of coals.

The development of procedures applicable to mixtures of known low molecular weight and to coals has taken place concurrently, many investigators contributing. Vlugter, Waterman, and van Westen[1] were among the first to apply a system of ring analysis to complex hydrocarbon mixtures. van Nes and van Westen[2] continued the study, developing the n-d-M method primarily for petroleum oils. Using refractive index, density, and elementary analysis, van Krevelen[3], van Krevelen and Chermin [4], and van Krevelen and Schuyer[5] developed a somewhat similar method of statistical analysis, applicable to coals and other substances where molecular weight could not be obtained. Smith[6] and Montgomery and Boyd[7] elaborated on both methods to obtain further structural parameters, testing the methods using data for a variety of pure hydrocarbon compounds as recorded by the American Petroleum Institute Research Project 42. Good agreement was obtained with respect to paraffins and naphthenes, but discrepancies were observed for the aromatics, particularly those consisting of fused rings. Dryden[8], working with coals, compared structural information derived from x-ray, nuclear magnetic resonance, and infrared data with comparable information calculated from the densimetric method of van Krevelen and found that agreement usually was poor.

Since the non-hydrocarbon constituents of the asphaltic fraction of crude oils and the insoluble organic residues obtained from ancient sediments, as well as of refinery asphalts, are believed to contain both aliphatic and aromatic fused ring groups, a re-investigation of the densimetric methods of ring analysis was considered justified.

(1) J. Inst. Petrol. Tech., 18, 735 (1932); Ibid., 21, 661 (1935).
(2) "Aspect of the Constitution of Mineral Oils," Elsevier, New York, 1951.
(3) Brenn. Chem., 34, 167 (1953).
(4) Fuel, 33, 79 (1954).
(5) "Coal Science," Elsevier, New York, 1957.
(6) Ohio State Univ. Bull., 152, 1 (1953).
(7) Anal. Chem., 31, 1290 (1959).
(8) Fuel, 37, 444 (1958).

For mixed aliphatic-aromatic compounds or mixtures thereof where the molecular weight could be determined, the following equations have been proposed by van Krevelen:

$$(1) \qquad \frac{M}{\rho} = \sum_i n_i V_i - K_M$$

where:

$$(2) \qquad K_M = V_R R$$

M = molecular weight of the compound or mixture,
ρ = the density,
n_i = the number of the i th atomic species,
V_i = Traube's atomic volumes,
K_M = molar volume contraction,
V_R = molar volume contraction per ring,
R = number of rings.

For aliphatic compounds or mixtures, K_M is approximately zero.

To cope with substances such as coal where molecular weight is very high or cannot be determined, the equation was converted to the form:

$$(3) \qquad \frac{1200}{\%C \cdot \rho} = \sum_i n_i V_i / C - V_R \cdot \frac{R}{C}$$

where %C is the per cent carbon obtained by elementary analysis and C is the number of carbon atoms in the structural unit.

To calculate the average number of rings per molecule, R, from equations (1) and (2) or the number of carbons per ring, C/R, from equation (3), it is necessary to evaluate V_R. Using three reference substances, namely, cellulose where R = 0, polystyrene where R = 1, and graphite where R = ∞ van Krevelen and Chermin derived the empirical relation:

$$(4) \qquad V_R = 9.1 - 3.6 \frac{H}{C}$$

where H is the number of hydrogen atoms.

Relations (1) and (3) thus become:

$$(5) \qquad R = \frac{9.9C + 3.1\,H + \ldots - \frac{M}{\rho}}{9.1 - 3.6 \frac{H}{C}}$$

and

$$(6) \qquad \frac{C}{R} = \frac{9.1 - 3.6 \frac{H}{C}}{9.9 + 3.1 \frac{H}{C} + \ldots - \frac{1200}{\%C \cdot \rho}}$$

Equation (6) was used to calculate the number of carbons per ring for a native asphaltene prepared in this laboratory from a Lagunillas crude oil and for two carbon blacks studied by Kuroda[9]. In Table I, Part A, the values obtained (underlined) are compared with values derived from infrared, nuclear magnetic resonance, and x-ray data. The numerical results indicate that the values of C/R calculated by means of equation (6) are too low.

(9) J. Colloid Sci., 12, 496 (1957).

Testing of equation (5) with compounds of known structure indicated that the expression for V_R, equation (4), probably was in error. That this relationship was empirical and disputable was recognized, of course, by van Krevelen. Rather than being a function of H/C, V_R appeared to be a constant for systems comprising three or more fused rings. To test the theoretical implications of this conclusion, an attempt has been made to derive from basic assumptions an expression for V_R.

In order to treat the problem of a condensed ring aromatic system, i.e., of a hexagonal network in two dimensions, it is necessary to assume some sort of model. A number of models are possible, e.g., a circle, exemplified by coronene; a square, by anthrodianthrene; a triangle, by perinaphthindene; and a rectangle, by perylene. For all these models, however, the number of rings can be expressed as a function of the number of aromatic carbon atoms and the number of aromatic hydrogen atoms by the equation:

$$R = 1 + \frac{C_A - H_A}{2} \tag{7}$$

where:

$$H_A = p\, C_A^{1/2} - q \tag{8}$$

In the latter equation the values of p and q vary with the model. Of the various possible models, the rectangular was selected for development of an expression for V_R.

If an aromatic cluster is designated as [m,n] according to the method of Coulson[10] where m denotes the number of biphenyl type rings, i.e., along the x axis, and n the number of naphthalene type rings, i.e., along the y axis, then:

$$H_A = 2(2m + n) \tag{9}$$

$$C_A = 2m(2n + 1) \tag{10}$$

and the number or rings as:

$$R = 2mn - m - n + 1 \tag{11}$$

Now, solving equation (11) in terms of H_A and C_A, equation (7) is obtained. Since long chains of condensed aromatic rings are seldom encountered in stable molecules, the simplified approximation is made that:

$$m \leq n \tag{12}$$

Now, H_A can be expressed in terms of C_A and after simplifying,

$$H_A = 3C_A^{1/2} - 3/2 \tag{13}$$

or

$$R = 0.5\, C_A - 1.5\, C_A^{1/2} + 1.75 \tag{14}$$

If the general equation (1) is applied to an aromatic cluster and the terms transposed,

$$K_M = \sum_i n_i V_i - M/\rho_A \tag{1a}$$

Substituting Traube's values for $\sum_i n_i V_i$ and the value of M:

$$K_M = 9.9C_A + 3.1H_A - (12C_A + H_A)\rho_A^{-1} \tag{15}$$

(10) "Proceedings of the Conference on Carbon," held at the University of Buffalo, Symposium Publication Division, Pergamon Press, New York, 1958.

To proceed further, it is necessary to evaluate ρ_A in terms of C_A. This step has been achieved through the following derivation -

In the case of a two-dimensional hexagonal net the area of the equilateral triangle formed by joining the centers of three adjacent rings can be expressed as:

$$(16) \qquad \Delta = 3\sqrt{3} \cdot a^2/4$$

If the net is comprised of aromatic carbon atoms, a is the bond distance and Δ the area occupied by one carbon atom. For a system consisting of uniformly stacked sheets, the minimum interlayer distance is 3.34 Å and hence the maximum density, 2.28 g./cm.^{3}.

Now it can be seen from Figure 1 that for aromatic hydrocarbons the density can be related to the number of carbon atoms by means of the equation:

$$(17) \qquad \frac{2.28}{\rho} - 1 = a\, C_A^{\,b} .$$

Although this equation is considered empirical at present, there appears to be theoretical evidence to support it. The plotted points in the figure represent nine aromatic hydrocarbons of known structure and the two carbon blacks cited in Table I, Part A. From the resulting straight line, the intercept, a, and the slope, b, can be evaluated as follows:

$$a = 3.15$$
$$b = -0.5$$

and equation (17) becomes:

$$(18) \qquad \rho_A^{-1} = 0.44 + 1.38\, C_A^{-1/2}$$

With an expression for ρ_A in terms of C_A, it is possible to continue development of the relationship expressed by equation (15). Substituting the values of H_A for equation (13) and ρ_A from equation (18), and dropping the small $C_A^{-1/2}$ term, equation (15) becomes:

$$(19) \qquad K_M = 4.6 \quad -8.6\, C_A^{1/2} \quad -8.1$$

The final objective is to eliminate C_A by combining equation (19) with equation (14) and to substitute the resulting value of K_M in the general equation (1). Owing to the form of equations (19) and (14), a general solution for K_M in terms of R is difficult. Accordingly, the operation was accomplished graphically in Figure 2 by substituting arbitrary values of C_A into the equations and solving for R and K_M. The plotted points represent actual values for ten polynuclear aromatic hydrocarbons. The curve will be seen to be a straight line at large values of R but to become slightly concave upward at low R and does not quite pass through the origin. The slight curvature and failure to pass through the origin, of course, are not consistent with condition that K_M must be zero at R equal to zero. This is merely the result of the simplifying approximations that have been made.

The foregoing derivation shows that the assumption of V_R equal to a constant is entirely reasonable. To obtain the value of the constant, it is necessary only to replace the derived curve by its limiting slope.

Hence:

$$(20) \qquad V_R = \frac{K_M}{R} = 9.2$$

Similar derivations based on the circular, square, and triangular models lead to equations for H_A differing only slightly from that for the rectangular model, equation (13), as follows:

$$(21) \quad \text{round} \qquad H_A = 2.46\, C_A^{1/2}$$

$$(22) \quad \text{square} \qquad H_A = 2.82\, C_A^{1/2} - 2$$

$$(23) \quad \text{triangular} \qquad H_A = 3\, C_A^{1/2} - 1$$

As can be seen, all these equations yield curves closely approximating that shown in Figure 2 for the rectangular model, thus confirming the generality of the conclusion that V_R should be a constant. Whatever the model chosen, the numerical value of the constant is the same.

On the basis of the above results, it is proposed that the following equations be used for substances containing condensed ring systems:

$$(24) \qquad R = 0.11\,(9.9\,C + 3.1\,H + \ldots - \frac{M}{\rho})$$

where molecular weight can be determined and by:

$$(25) \qquad \frac{C}{R} = \frac{9.2}{9.9 + 3.1\,H/C + \ldots - \frac{1200}{\%C \cdot \rho}}$$

for substances where molecular weight cannot be determined.

In Table I, Part B, are presented new values of C/R for the petroleum asphaltene and carbon blacks, cited in Table I, Part A, this time calculated by means of equation (25). Referring to Part A, it will be seen that the values are in better agreement with the values derived from infrared, nuclear magnetic resonance, and x-ray than the values calculated by means of van Krevelen's equation (6).

In Table I, Part C, the values of C/R calculated by the two alternate methods are listed for the above asphaltene and for two others prepared from crude oils of widely different geographic origin. Values of density and elementary analysis are provided for comparison. It will be seen that the values of C/R computed by the method of van Krevelen and Chermin and by the modified method derived in this paper deviate not only in absolute value but also in trend. Further, it is interesting to note that the values of C/R calculated by the modified method do not vary as much with density and elementary analysis as do the values obtained by means of the van Krevelen equation, nor is there a direct correlation with density or the percentage of any single element.

In Tables II and III, equation (24) has been used to calculate values of R for a variety of compounds of known structure, using density values from the literature and values of C, H, etc., from the formulas. The compounds in Table II are unsubstituted aromatic hydrocarbons containing condensed ring systems. The compounds in Table III in many instances contain hetero elements and range from

aliphatic to cyclic systems containing substituted saturated and aromatic ring systems. The good agreement between the calculated R values and those indicated by the formulas is evident. It is concluded, therefore, that equation (25) will be dependable when applied to complex substances such as asphaltic fractions of crude oils and the black insoluble organic fraction of ancient sedimentary rocks.

Acknowledgment

This work was sponsored by the Gulf Research & Development Company as a part of the research program of the Multiple Fellowship on Petroleum.

Table I

Values of C/R for
A Native Petroleum Asphaltene and Two Commercial Carbon Blacks

Part A

Comparison of the
Values Calculated by Means of the van Krevelen and Chermin Equation (6)
with
Values Obtained from Other Physical Measurements

Substance	Data From	Method	C/R Calculated
Asphaltene (Lagunillas)	infrared spectroscopy[1]	absorbance of the C-H stretching	5.7
	nuclear magnetic resonance[1]	proton type area	5.5
	x-ray[1]	(γ) and (002) bands	5.9
	x-ray[1]	(10) and (11) bands	4.2
	density-elementary analysis[1]	densimetric (van Krevelen and Chermin) Equation (6)	3.5
Royal Spectra	x-ray[2]	(10) band	2.9[3]
	density - H/C approximated from X-ray L_a values[2]	densimetric Equation (6)	2.1
Statex B	x-ray[2]	(10) band	2.6[3]
	density - H/C approximated from x-ray L_a values[2]	densimetric Equation (6)	2.1

Part B

Values Calculated by Means of Equation (25) Derived by the Authors

Substance	Data From	C/R Calculated
Asphaltene (Lagunillas)	density-elementary analysis	6.2
Royal Spectra	density - H/C approximated from x-ray L_a values [2]	2.5
Statex B	density - H/C approximated from x-ray L_a values[2]	2.3

Part C

Density, Elementary Analysis, and Values of C/R for Three Asphaltenes
Prepared from Crude Oils of Widely Different Geographic Origin

Field	Location	Helium Density ρ	Elementary Analysis Per Cent C	H	O*	N	S	C/R Calculated by Means of Equation (6)	(25)
Lagunillas	Western Venezuela	1.158	84.2	7.9	1.6	2.0	4.8	3.46	6.24
Wafra	Neutral Territory (Middle East)	1.164	81.8	8.1	1.5	1.0	7.8	3.14	5.90
Baxterville	Mississippi U.S.A.	1.172	84.5	7.4	1.7	0.8	5.6	3.62	6.19

1 Measurements made in this laboratory.
2 Taken from the work of Kuroda, H., J. Colloid Sci., 12, 496 (1957).
3 Calculated assuming all the carbons are contained in a condensed aromatic sheet.

* Direct determinations

Table II
Calculation of R for
Compounds Consisting of Condensed Aromatic Ring Systems

Compound	Formula	Molecular Weight M	Density ρ	K_M	Rings per Molecule, R: Theoretical From Formula	Rings per Molecule, R: Calculated by Equation (24)
naphthalene	$C_{10}H_8$	128	1.152[1]	12.7	2	1.4
anthracene	$C_{14}H_{10}$	178	1.25[1]	27.2	3	3.0
fluorene	$C_{13}H_{10}$	166	1.203[2]	21.7	3*	2.4
triphenylene	$C_{18}H_{12}$	228	1.302[1]	40.3	4	4.4
chrysene	$C_{18}H_{12}$	228	1.274[1]	36.2	4	4.0
perylene	$C_{20}H_{12}$	252	1.35[1]	48.5	5	5.3
anthanthrene	$C_{22}H_{12}$	276	1.39[3]	56.4	6	6.2
coronene	$C_{24}H_{12}$	300	1.377[4]	57.0	7	6.3
ovalene	$C_{32}H_{14}$	398	1.477[5]	90.7	10	10.0
circumanthracene	$C_{40}H_{16}$	496	1.52[6]	119	13	13.1

* Contains one five-membered ring.

1. "The Merck Index of Chemicals and Drugs," 6th Ed., Merck and Co., Inc., Rahway, New Jersey, 1952.
2. Lange, N.L., "Handbook of Chemistry," 9th Ed., Handbook Publishers, Sandusky, Ohio, 1956.
3. J. G. White, J. Chem. Soc., 1948, 1398.
4. J. M. Robertson and J. G. White, Nature, 154, 605 (1944).
5. D. M. Donaldson and J. M. Robertson, Proc. Roy. Soc., A220, 157 (1953).
6. E. Clar, et al.,J. Chem. Soc., 1956, 3876.

Table III
Calculation of R for
Compounds of Varying Structure and Elementary Composition

Compound	Formula	Molecular Weight M	Density ρ	Rings per Molecule: Theoretical From Formula	Rings per Molecule: Calculated by Equation (24)
d-tartaric acid	$C_4H_8O_6$	150	1.759[1]	0	0
hexachloroethane	C_2Cl_6	237	2.09[2]	0	0
borneol	$C_{10}H_{18}O$	154	1.011[2]	1	0.7
p-hydroxybenzoic acid	$C_7H_6O_3$	138	1.46[2]	1	0.5
anthraquinone	$C_{14}H_8O_2$	208	1.43[2]	3	2.8
α-naphthylphenylmethane	$C_{17}H_{14}$	218	1.165[3]	3	2.7
papaverine	$C_{20}H_{21}NO_4$	339	1.337[4]	3	2.8
rosin	$C_{20}H_{29}O_2$	302	1.095[5]	3	2.5
laudanine	$C_{20}H_{25}NO_4$	243	1.26[2]	3	2.1
α-progesterone	$C_{21}H_{30}O_2$	314	1.166[2]	4	4.2
20-methylcholanthrene	$C_{21}H_{16}$	268	1.28[2]	5	4.2
strychnine	$C_{21}H_{22}N_2O_2$	334	1.359[4]	5	4.5

1. Bailey,T.,"Bailey's Chemists' Pocket Book," 20th Ed.,E.and F.N.Spon.,Ltd.,London,1948.
2. "The Merck Index of Chemicals andDrugs," 6th Ed.,Merck and Co., Inc., Rahway, New Jersey, 1952.
3. Egloff,G.,"Physical Constants of Hydrocarbons," Vol.4,Reinhold Publishing Corp., New York, 1947.
4. Hodgman, C. D., et al., "Handbook of Chemistry and Physics," 41st Ed., Chemical Rubber Publishing Company, Cleveland, 1959.
5. Simonds, H. R., et al., "Handbook of Plastics," 2nd Ed., D. Van Nostrand Company, Inc., New York, 1949.

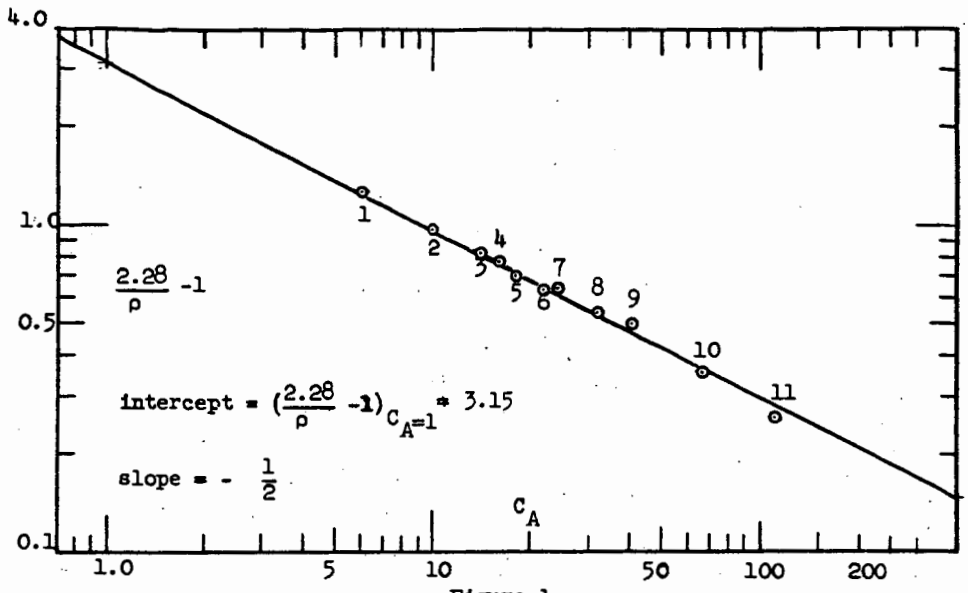

Figure 1

Relation of Density to Aromatic Carbon Number

(1) Benzene (2) Naphthalene (3) Anthracene (4) Pyrene
(5) Triphenylene (6) Anthanthrene (7) Coronene (8) Ovalene
(9) Circumanthracene (10) Royal Spectra (11) Statex B

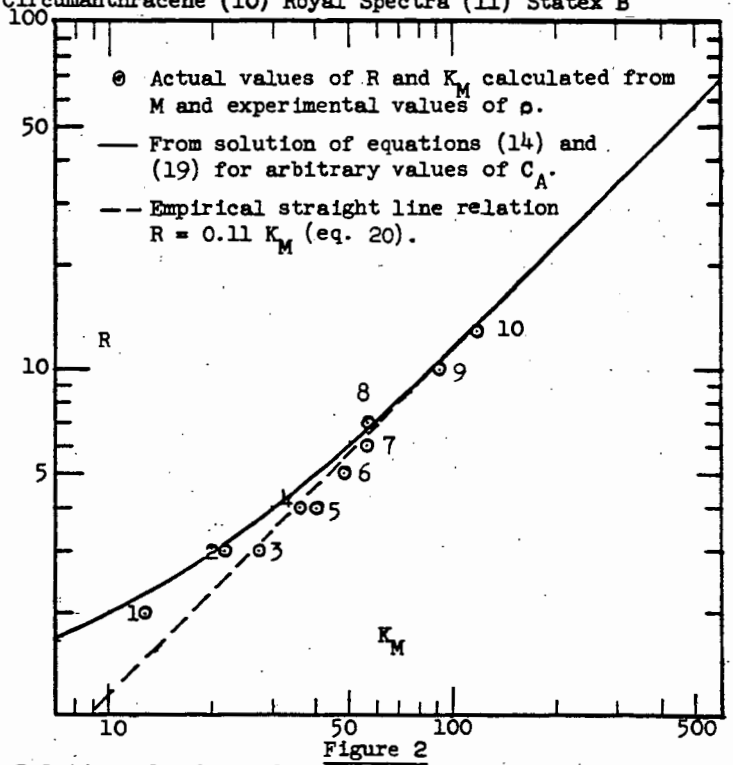

Figure 2

Relation of Molar Volume Contraction and Ring Number

(1) Naphthalene (2) Anthracene (3) Fluorene
(4) Chrysene (5) Triphenylene (6) Perylene
(7) Anthanthrene (8) Coronene (9) Ovalene
(10) Circumanthracene

CATALYTIC STEAM REFORMING OF LIGHT LIQUID HYDROCARBONS

J. C. Yarze and T. E. Lockerbie

The M. W. Kellogg Company
Research and Development Department
Jersey City, New Jersey

Introduction

In the chemical process industry, catalytic steam-hydrocarbon reforming of natural gas or propane is widely employed to produce ammonia synthesis gas, high-purity hydrogen, and hydrogen-carbon monoxide mixtures for chemical synthesis. Currently, synthetic ammonia plants based on natural gas reforming account for 70-80 per cent of all ammonia produced in the United States, and a large percentage of domestic synthetic methanol production is derived from steam-hydrocarbon reforming.

The manufactured gas industry also employs steam-hydrocarbon reforming in the production of low-Btu carrier gas. Several continuous reforming units employing natural gas or propane feedstocks and steam-air oxidizing mixtures have been built in the United States. In a typical application, carrier gas and natural gas are blended to provide a mixture with the heating value, specific gravity, and hydrogen content required for satisfactory performance in customers' appliances. In Europe and Asia, carrier gas from steam-hydrocarbon reforming is commonly enriched with light hydrocarbons and diluted with inerts to about 0.5 specific gravity and 400-500 Btu higher heating value. The resulting mixture is used as a supplement or replacement for coke oven-carburetted water gas mixtures.

Steam-natural gas or steam-propane reforming techniques employed in producing ammonia synthesis gas, Fischer-Tropsch synthesis gas, hydrogen, and carrier gas have been described elsewhere /2,3,4,5,8/. In these and other applications of conventional fired-tube reforming furnaces, certain similarities are apparent. Feedstocks require careful desulfurization prior to conversion if temporary poisoning of nickel reforming catalyst and shutdowns for catalyst regeneration are to be avoided. Within the catalyst tubes, conversion of the original steam-hydrocarbon mixture occurs via highly endothermic chemical reactions yielding a product containing hydrogen, carbon monoxide, carbon dioxide, and small amounts of methane. When injection of air to the reformer is practiced, nitrogen becomes an additional component of the product. At the tube outlet, where gas temperatures of 1550°F may be obtained, product distribution is largely governed by equilibrium considerations. The water gas shift reaction

$$H_2O + CO \rightleftharpoons H_2 + CO_2 \qquad (1)$$

is found to be at equilibrium in reformer effluent, while the steam-methane reaction

$$H_2O + CH_4 \rightleftharpoons 3H_2 + CO \qquad (2)$$

attains a close approach to equilibrium.

Deposition of carbon on catalyst located near the tube inlet can be an operational problem in fired-tube reformers. Avoidance of carbon deposition is required to ensure long periods of continuous operation and prevent severe catalyst spalling. Freedom from carbon deposition is obtained by employing active catalysts

at high temperatures, and by using more than stoichiometric quantities of steam. Relative amounts of steam and hydrocarbon in the original mixture are conveniently specified by the steam-carbon ratio, moles steam per feedstock carbon atom. Selection of the optimum steam-carbon ratio is an important function of reformer design. Sufficient excess steam must be employed to prevent costly shutdowns and resulting lost production. However, a plant designed for an excessively high steam-carbon ratio also results in high manufacturing costs, since both investment and operating costs increase with increasing steam-carbon ratio.

Although continued growth of reforming capacity based on natural gas and propane feedstocks is predicted, an increased interest in utilizing heavier feedstocks has recently been indicated. In this paper, results of pilot plant and exploratory reforming tests on light liquid hydrocarbons are described and related to the known behavior of natural gas and propane. Particular consideration is given to the economically important steam-carbon ratio variable.

Pilot Plant Experiments

A. Apparatus and Methods

A vertically mounted 1-inch reformer heated by a conventional electrical resistance furnace was used for screening of variables and determination of operability limits at 20-125 psig reforming pressure. The reactor consisted of a 57-3/4 inch length of 1-inch Inconel pipe. A catalyst support tray at the tube outlet and an axial thermowell extending the length of the reactor were provided. Attached to the upper or inlet end was a 2-inch welding-neck flange. The inner diameter of the flange provided surface for falling-film evaporation of water, and the annulus formed by the inner diameter of the flange and the outer diameter of the tube afforded volume for hydrocarbon vaporization and mixing of vaporized water and hydrocarbon. A preheater assembly, 28 inches of 316 stainless steel bar stock welded to a 2-inch blind flange, fitted snugly into the reactor, with 0.003 inches radial clearance. The flange and bar stock were suitably tapped for inlet connections and the axial thermowell, and the bar stock was threaded to provide heat transfer area. A stainless steel ring closure was employed. Catalyst bed depth was 30 inches.

In operation, water and hydrocarbon were pressured from calibrated feed tanks with nitrogen. Flow rates were controlled by small air-operated valves responding to pressure drops across hypodermic needle orifices. Water and hydrocarbon metered to the reactor inlet were vaporized in the falling-film evaporator section of the reactor, preheated by downward passage through the preheater spiral, and contacted with catalyst. Furnace windings opposite the vaporization, preheat, and reaction sections of the reactor were automatically controlled. Reaction products were cooled by indirect exchange, and unreacted water separated. Product gases flowed through a back-pressure regulator maintaining unit pressure to a wet-test meter, sampling manifold, and vent. Periodic samples were analyzed by mass spectrometer. Pressure drop across the catalyst bed was continuously measured by a differential pressure cell with a range of 0-100 inches of water.

In all experimental studies made in the 1-inch unit, 1/8 inch extrusions of commercial steam-hydrocarbon reforming catalyst were utilized to maintain a reasonable relationship between reactor diameter and catalyst size. The particular catalyst employed was a pre-shrunk preparation which contains 20-25 per cent by weight nickel (as NiO) uniformly distributed throughout each pellet. Fresh catalyst, containing 0.49 per cent by weight sulfur, was either pretreated extensively at high temperature with a steam-hydrogen mixture, or used in extended reforming runs at high steam-carbon ratios, until the catalyst sulfur content was reduced to 0.003-0.005 per cent by weight. Extensive pretreatment was mandatory, since unreliable results were obtained with catalysts containing as little as 0.01 per cent by weight sulfur.

Feedstocks employed were of 99+ mole per cent purity, containing a maximum of 5 parts per million sulfur by weight. Catalysts discharged after extended contact with feedstocks containing 5 parts per million sulfur uniformly analyzed 0.003-0.005 per cent by weight sulfur, indicating that the sulfur content of the catalyst was substantially constant during test periods.

After catalyst pretreatment, feedstocks were reformed in a series of 12 or 24 hour experiments conducted at progressively lower steam-carbon ratios. Testing was continued until an increase in reactor pressure drop was indicated by the differential pressure cell. A measurable increase in pressure drop was taken as evidence of carbon formation in the catalyst bed at the particular steam-carbon ratio employed.

B. Experimental Results

For orientation, the reforming chacteristics of 99.7 mol per cent cylinder propane were initially investigated, employing the technique described above. Typical experimental data obtained at 125 psig reforming pressure and substantially commercial temperatures and hydrocarbon space velocities are presented in Table 1. Tests made at steam-carbon ratios ranging from 3.77 to 1.51 were completed without evidence of carbon deposition. At 1.35 steam-carbon ratio, catalyst activity gradually declined during 24 hours of operation, and reactor pressure drop increased about 0.4 inches per hour. This behavior was interpreted as arising from deposition of carbon on the catalyst. Additional data from tests made without nitrogen diluent and a correlation relating rate of pressure drop increase to steam deficiency indicate that 1.50 moles of steam per carbon atom are required for operability at 125 psig when reforming propane.

Wet product gas analyses permit calculation of apparent gas temperatures at the tube outlet, assuming that the water gas shift and steam-methane reactions are at equilibrium in the product. Results of these calculations are presented in Table 1. The assumption of equilibrium for either reaction gives outlet temperatures which are generally in reasonable agreement with the measured outlet temperature. In larger pilot plants, the steam-methane reaction is usually further removed from equilibrium. The close approach of the steam-methane reaction to equilibrium at the outlet of the 1-inch unit reflects the high activity of 1/8-inch catalyst pellets relative to commercial-sized pellets when both are employed at the same hydrocarbon space velocity.

A similar operability study was made on ASTM grade n-heptane, a representative light liquid hydrocarbon reforming feedstock. Results of these tests are also presented in Table 1. At 20 psig reforming pressure and commercial temperatures and hydrocarbon space velocities, reactor pressure drop did not increase during test periods at 3.03 steam-carbon ratio and higher. At 2.53 steam-carbon ratio, reactor pressure drop increased 0.4 inches per hour during 12 hours of steady operation. Additional tests confirm that, at 20 psig, about 3.0 moles of steam per carbon atom are required to prevent carbon deposition when reforming n-heptane.

Product gas ratios and calculated outlet temperatures obtained when reforming n-heptane closely resemble results obtained using propane feedstock. Except that higher steam-carbon ratios are required for operability, the reforming characteristics of n-heptane appeared to be fundamentally similar to those of propane.

C. Effect of Hydrocarbon Molecular Weight on Operability

Operability limits determined for propane and n-heptane in this study can be compared with operability data from the literature /7/ to provide an estimate of the relationship between hydrocarbon molecular weight and minimum operable steam-carbon ratio at several reforming pressures. In Figure 1, published data obtained

in a 5-inch tube at essentially atmospheric pressure are compared with data from this study. A single relationship appears to represent both sets of data adequately. Required steam-carbon ratio is shown to increase logarithmically with increasing molecular weight at several pressures. The rate of increase is moderate, operability limits ranging from 1.1 steam-carbon ratio for natural gas or methane to 3.0 steam-carbon ratio for n-heptane.

While agreement between the two sets of data may be partly fortuitous, owing to differences in feedstock purity, catalysts, and operating conditions, additional studies in the 1-inch pilot plant tend to confirm the relationship shown in Figure 1. When reforming olefin-free and sulfur-free hydrocarbons, reforming pressures ranging from 20 to 125 psig are found to have no significant effect on minimum steam-carbon ratio.

Study of Reforming Variables in Glassware

A. Apparatus and Methods

Since pilot plant tests indicated no major effect of pressure on minimum steam-carbon ratios when reforming olefin-free and sulfur-free hydrocarbons, the study of light liquid hydrocarbon reforming was continued in glassware at atmospheric pressure to further clarify the influence of reactor and feedstock variables on operability. Reactions of steam-hydrocarbon mixtures were studied over various commercial reforming catalysts at several temperatures and steam-carbon ratios in a conventional 1-inch diameter quartz reactor heated by an electrical resistance furnace. A 2-inch bed of catalyst was employed so that, in effect, the top portion of a full catalyst charge in the 1-inch pilot plant was being studied, this being the critical zone for carbon formation.

In operation, hydrocarbon feedstock was introduced from a pressured container and vaporized. Flow rate to the glass unit was measured by calibrated rotameters. Steam-carbon ratio was controlled by gas saturation. A metered stream of vaporized feedstock, saturated to the desired steam-carbon ratio, was preheated by rapid passage through an annulus formed by the inner tube wall and snugly fitted quartz plug, and contacted with catalyst. Reactor effluent was rapidly removed from the reaction zone through 3-millimeter tubing, cooled to condense unreacted steam, measured in a wet-test meter, and vented. Periodic product gas samples were withdrawn and analyzed by mass spectrometer. Feedstock conversion was varied by altering hydrocarbon space velocity at constant steam-carbon ratio and temperature. At the completion of each test, the catalyst charge was analyzed for carbon by combustion and absorption of carbon dioxide. Previously cited limitations on catalyst and feedstock sulfur contents were observed. While the apparatus and technique employed are not ideally suited for kinetic measurements, they permit very efficient screening of variables for large effects on operability and product distribution.

Before any reforming experiments were made, the catalyst space was filled with quartz chips, and steam-hydrocarbon mixtures passed through the unit at various combinations of temperature and contact time. In this way, temperature-contact time combinations sufficient to cause thermal cracking were determined for all feedstocks. Subsequent reforming tests were then carried out at conditions where precracking of feedstock could not occur, thus ensuring that catalytic reactions alone were being investigated.

In the tests to be described, two commercial catalysts were employed. Catalyst A is an impregnated type, containing about 5 per cent nickel (as NiO) on alumina. Catalyst B is the compounded preparation previously used for studies in the 1-inch pilot plant.

B. Experimental Results

Typical data obtained when reforming 99.7 mole per cent n-butane to partial conversion at 1075°F or 1275°F and 3.0 steam-carbon ratio are presented in Table 2. At all conversion levels, dry product gases are observed to consist almost entirely of conventional reformed products and unreacted feedstock. Various olefinic and paraffinic butane decomposition products are present at low concentrations in all product gas samples. Methane, a final product in commercial reforming operations, is not detected in gases produced at low conversions of feedstock. These characteristic features of partially reformed gases are confirmed by other studies employing different temperatures, steam-carbon ratios, and catalysts.

Product ratios corresponding to equilibrium constants for the water gas shift reaction

$$H_2O + CO \rightleftharpoons H_2 + CO_2 \qquad (1)$$

and steam-methane reaction

$$H_2O + CH_4 \rightleftharpoons 3\ H_2 + CO \qquad (2)$$

have been calculated and are reported in Table 2. At 1275°F, the water gas shift equilibrium constant is approximately 1.61. Shift constants calculated from experimental data obtained with compounded Catalyst B show a strong dependency on the extent of n-butane conversion. At conversions below 10 per cent, the shift reaction is far removed from equilibrium. However, in the range of 10-30 per cent n-butane conversion, equilibrium is rapidly approached, while at still higher conversions, equilibrium constants appear to scatter about the equilibrium value. At 1075°F, where the shift equilibrium constant is approximately 2.85, a parallel trend is evident from data obtained using Catalyst B. Data obtained with impregnated Catalyst A at 1275°F, indicate a much slower approach to equilibrium than with Catalyst B. However, the reproducibility of this apparent difference in catalyst activity for the shift reaction has not been determined. In general, all data in Table 2 indicate that the water gas shift reaction rapidly proceeds towards equilibrium in the presence of nickel reforming catalysts. Similar conclusions are made in a published study on natural gas reforming /6/.

The equilibrium constant for the steam-methane reaction at 1275°F is approximately 9.5. Calculated steam-methane equilibrium constants in Table 2 indicate that the approach to equilibrium over both Catalysts A and B, is very slow for this reaction, even at high n-butane conversions. This result is in agreement with commercial steam-hydrocarbon reforming results, where equilibrium is approached but not attained at much higher contact times than were employed in this study.

Methane production is further analyzed in Table 2 as a function of n-butane conversion at 1075°F or 1275°F and 3.0 steam-carbon ratio. In Figure 2, tabulated mole ratios of methane produced to n-butane converted are plotted against conversion and extrapolated towards zero conversion to determine if methane is a primary reaction product. As Figure 2 indicates, methane is produced only when the conversion of n-butane exceeds about 15 per cent. The relationship obtained appears to be essentially independent of catalyst type or temperature. Thus, methane is not a primary product of steam-butane reforming, and does not arise directly from catalytic decomposition of feedstock.

Consideration of other possible reactions yielding methane indicates that methane is probably formed by the methanation reaction

$$3\ H_2 + CO \rightleftharpoons H_2O + CH_4 \qquad (3)$$

which is catalyzed by nickel at conditions similar to those employed in reforming. Production of methane is limited by the steam-methane back-reaction, since methane molecules can disappear by successfully competing with unreacted n-butane for active reforming sites on the catalyst.

Analyses of discharged catalysts indicate that, at steady state conditions, detectable amounts of carbon are always present on active catalysts. In general, carbon contents are higher at the lower reforming temperatures. Compounded Catalyst B contains less carbon than impregnated Catalyst A after comparable periods of exposure to steam hydrocarbon mixtures. The temperature dependency of catalyst carbon content is illustrated specifically in Table 3, where carbon levels are compared for runs made with Catalyst B at nominally constant conversion, constant steam-carbon ratio, and 900°F, 1100°F and 1300°F. Although absolute values for carbon content may be specific for the apparatus and conditions employed, these analyses indicate that carbon content decreases almost exponentially with increasing temperature.

All data from tests on n-butane have been evaluated to determine the apparent kinetics of n-butane disappearance. While the data are not sufficiently precise for a detailed kinetic analysis, the rate of butane disappearance appears to be approximately proportional to n-butane concentration for the temperatures, steam-carbon ratios, and catalysts studied. The apparent first order reaction rate constant increases exponentially with temperature. First order kinetics have also been shown to apply in natural gas reforming /1/. A comparison of rate constants for butane disappearance by steam-hydrocarbon reforming and by thermal cracking indicates that the reforming reaction is roughly 100 times faster at the same temperature, thus confirming that thermal cracking is not a major reaction in reforming.

Discussion

Information developed from partial conversion and pilot plant studies permits some reasonable speculation on the individual chemical reactions occuring in steam-hydrocarbon reforming. The overall conversion of paraffin hydrocarbons and steam to reformed products is indicated as occurring through a complex series of consecutive and competing reactions. Hydrocarbon molecules diffuse to the catalyst surface, are adsorbed, and undergo catalytic cracking-dehydrogenation reactions which yield strongly absorbed olefinic fragments. Further dehydrogenation-polymerization reactions occur, leading to formation of coke or carbon on the catalyst. The sum of these consecutive steps is an overall reaction in which feedstock molecules are converted to carbon on the catalyst at a rate proportional to feedstock concentration.

Carbon deposits are continuously removed from the catalyst by a competing reaction involving steam. Adsorbed steam molecules react with deposited carbon to form hydrogen and carbon monoxide or carbon dioxide. These products, hydrogen evolved in the cracking-dehydrogenation-polymerization step, and steam also participate in methanation and water gas shift side reactions. In addition, a portion of the methane produced by methanation is continuously reformed through a sequence similar to that followed by the original feedstock.

This qualitative mechanism is helpful in rationalizing the behavior of reforming units, since it predicts that net carbon formation and inoperability result when the rate of feedstock decomposition exceeds the rate of carbon removal by the steam-carbon ratio. Operable reforming units are thus characterized by equal rates of carbon formation and removal at all points in the catalyst bed. Any change in conditions which induces a relative increase in the rate of carbon removal from the catalyst will accordingly favor operability. Major operating variables capable of altering this relative rate are temperature and steam-carbon ratio. An

increase in catalyst bed temperature will, in general, favor the attainment of operability. Although the rates of reactions producing and removing carbon both appear to increase exponentially with temperature, the steam-carbon reaction rate apparently increases at a relatively greater rate, as demonstrated by catalyst carbon analyses. With all other reactor variables held constant, an increase in catalyst temperature will therefore increase the relative rate at which carbon is removed from catalyst at all points within the bed, or lower the equilibrium carbon content of catalyst.

An increase in steam-carbon ratio will also favor the attainment of operability by reducing the rate of hydrocarbon decomposition. When reforming n-butane, for example, an increase in steam-carbon ratio from 2.0 to 3.0 reduces butane concentration in the feedstock from 0.111 to 0.0796 mol fraction, a decrease of about 31 per cent. Thus the initial rate of butane decomposition to carbon near the tube inlet is decreased about 31 per cent. The corresponding slight increase in steam concentration, from 0.889 to 0.922 mol fraction, does not appear to greatly influence the rate of carbon-removing reactions. Small increases in steam concentration can therefore strongly influence the relative rates of carbon laydown and removal on catalyst located near the bed inlet.

These observations are consistent with operating experience in pilot plants and commercial units. Carbon deposition generally occurs near the tube inlet where catalyst temperatures are low; in this critical zone, the steam-carbon reaction proceeds slowly relative to decomposition. The effectiveness of increased steam-carbon ratio in suppressing carbon formation in the critical zone is well known.

The relationship between paraffin hydrocarbon molecular weight and minimum steam-carbon ratio presented in Figure 1 may also be a consequence of changes in the relative rates of competing reactions producing and removing carbon. Experience suggests that, at the same temperature and steam-carbon ratio, n-butane is catalytically decomposed to carbon more rapidly than methane. If the rate of reaction between steam and carbon is similar in both cases, net carbon formation or inoperability will be favored for the heavier feedstock. To attain an equal degree of operability, additional steam will be required to reduce the rate of n-butane decomposition to carbon. Hence n-butane will require a higher minimum steam-carbon ratio than methane to balance carbon production and removal. The relationship shown in Figure 1 may therefore arise from a regular increase in the rate of catalytic decomposition to carbon with increasing feedstock molecular weight.

Conclusions

Pilot plant tests demonstrate that presently available steam-hydrocarbon reforming catalysts can be used successfully with light liquid hydrocarbon feedstocks. The similarity of behavior and results noted in tests with propane and n-heptane indicate that light liquid hydrocarbons and currently reformed feedstocks follow a similar reaction path. Partial conversion experiments suggest a mechanism involving simultaneous catalytic conversion of feedstock to carbon and catalytic removal of carbon by the steam-carbon reaction. Water gas shift, methanation, and steam-methane reforming side reactions are additionally indicated as occurring on the catalyst. The qualitative mechanism presented appears to rationalize some observed effects of reforming temperature and steam-carbon ratio on operability.

Table 3

EFFECT OF REFORMING TEMPERATURE ON CARBON CONTENTS OF DISCHARGED CATALYSTS

Temperature, °F.	900	1100	1300
Carbon on Catalyst, Wt. %	1.34	0.46	0.12

REFERENCES

1. Akers, W.W. and Camp, D.P., "Kinetics of the Methane-Steam Reaction", A.I.Ch.E. Journal 1, 471-475 (1955).

2. Aron, "Kellogg Ammonia Process", Pet. Ref. 33, 3, 150 (1954).

3. Barnes, J.M. and Berger, E.S. "Eastern Utility Installs Catalytic Reforming Units", Gas 33, 39-42 (1957) December.

4. Eickmeyer, A.G. and Harshall, W.H., Jr., "Ammonia Synthesis - Gas Generation by Pressure Reforming of Natural Gas", Chem. Eng. Progr. 51, 418-421 (1955).

5. Reitmeier, R.E., Atwood, K., Bennett, H.A., Jr., and Baugh, H.M., "Production of Synthesis Gas by Reacting Light Hydrocarbons with Steam and Carbon Dioxide", Ind. Eng. Chem. 40, 620-626 (1948).

6. Riesz, C.H., Dirksen, H.A., and Pleticka, W.J., "Improvement of Nickel Cracking Catalysts", Institute of Gas Technology Research Bulletin No. 20, (1952) October.

7. Riesz, C.H., Jurie, P.C., Tsaros, C.L., and Pettyjohn, E.S., "Pilot Plant Catalytic Gasification of Hydrocarbons", Institute of Gas Technology Research Bulletin No. 6 (1953) July.

8. Updegraff, N.C., "Need Hydrogen? Examine This Process", Pet. Ref. 38, 9, 175-178 (1959).

Table 1

RESULTS OF PILOT PLANT REFORMING
TESTS ON PROPANE AND HEPTANE

Feedstock	C_3H_8						$n\text{-}C_7H_{16}$					
Test Duration, hr	20	24	24	24	24	24	24	12	12	22-1/4	12	12
Steam-Carbon Ratio, moles steam per carbon atom	3.77	2.85	2.28	1.83	1.51	1.36	8.35	6.41	3.98	3.89	3.03	2.53
Reactor Inlet Temperature, °F	710	640	670	650	685	650	720	730	810	805	795	805
Reactor Outlet Temperature, °F	1450	1430	1440	1445	1440	1455	1455	1445	1450	1435	1400	1400
Reactor Outlet Pressure, psig	126	125	126	125	126	125	20	21	20	20	20	20
Rate of Reactor Δp Increase, in. water per hr	0.0	0.0	0.0	0.0	0.0	0.4	0.0	0.0	0.0	0.0	0.0	0.4
Dry Product Gas Analysis, mole %												
CO	12.2	14.1	15.0	19.1	19.3	19.8	7.3	9.2	14.4	14.6	15.9	18.9
CO_2	10.7	9.6	7.7	5.6	5.1	4.3	18.2	17.0	12.7	12.4	10.7	9.4
H_2	64.0	61.2	59.6	56.7	57.2	57.0	74.5	73.8	72.9	73.0	73.3	71.6
CH_4	1.3	3.7	3.9	2.9	4.7	4.5/2/	-	-	-	-	0.1	0.1
N_2 /1/	11.8	11.4	13.8	15.7	13.7	14.4						
Atomic Balances, %												
C	104.3	101.7	102.0	102.0	100.7	100.0	101.4	95.1	96.3	95.3	96.5	98.2
H	100.2	98.3	99.5	94.3	93.8	97.3	106.2	99.5	97.1	96.3	105.6	101.2
O	99.5	100.8	95.9	96.9	91.5	91.2	106.0	99.9	98 3	94.1	101.7	98.0
N	103.2	87.9	109.8	120.3	99.4	99.7						
Outlet Temperature Calc. from Water Gas Shift Constant, °F	1490	1500	1495	1545	1515	-	1450	1440	1520	1515	1420	1455
Outlet Temperature Calc. from Steam-Methane Constant, °F	1470	1435	1460	1390	1510	-	-	-	-	-	-	-

/1/ Nitrogen diluent from feedstock.
/2/ At start of test period. Severe catalyst deactivation was noted during test.

FILE NO. E-3114
JCY:LA 11/12/59

Table 2

PARTIAL CONVERSION REFORMING OF BUTANE AT ATMOSPHERIC PRESSURE

Catalyst Designation	B	B	B	B	B	B	B	B	B	A	B	A	B	A	B	A	B
Temperature, °F	1065	1070	1070	1070	1070	1070	1070	1280	1275	1275	1275	1275	1270	1270	1275	1275	1275	1275
Methane Equivalent Space Velocity, std cu ft/ cu ft catalyst-hr	24,100	24,200	11,000	6,190	4,510	2,320	2,980	40,700	25,400	18,000	15,100	13,300	17,600	10,100	7,670	6,120	5,320	2,470	2,420
Steam-Carbon Ratio, moles steam per carbon atom	3.0	3.0	3.0	3.0	3.0	3.0	3.0	3.0	3.0	3.0	3.0	3.0	3.0	3.0	3.0	3.0	3.0	3.0	3.0
Feedstock Conversion, %	1.8	2.0	3.8	9.7	12.1	18.9	20.4	6.8	10.0	14.3	16.0	19.9	22.8	32.8	36.4	50.1	57.2	62.5	74.2
Dry Product Gas Analysis, mole %																			
CO	0.3	0.7	1.0	1.7	2.5	3.3	3.0	3.7	1.3	7.3	4.3	7.0	3.0	7.8	4.0	8.2	5.7	12.3	2.6
CO_2	3.7	4.8	7.2	12.8	14.3	14.9	15.4	8.1	10.9	8.8	13.0	10.6	13.1	11.8	13.9	13.5	13.5	11.3	14.1
H_2	15.3	19.0	29.3	49.9	50.7	60.1	60.6	36.8	54.0	55.2	54.2	61.4	62.7	63.6	65.4	68.3	72.5	66.2	78.8
CH_4	0.2	-	T /1/	0.2	-	0.8	0.7	-	-	-	-	0.7	2.2	2.1	1.2	3.2	3.7	5.3	2.7
C_2H_2	0.2	-	-	-	-	-	0.1	0.1	-	0.1	0.1	0.1	0.1	0.5	0.1	T /1/	-	-	-
C_2H_4	0.1	-	0.1	-	0.1	-	0.1	0.1	T /1/	0.2	0.1	0.1	0.1	0.1	0.1	0.1	T /1/	0.1	0.1
C_2H_6	0.2	0.1	0.1	-	-	-	0.1	0.3	0.3	0.5	0.3	0.2	0.3	0.7	0.2	0.2	0.1	0.3	T /1/
C_3H_6	-	-	0.2	-	0.1	-	0.1	0.3	0.4	-	0.6	-	0.4	0.1	0.2	-	0.1	-	T /1/
C_3H_8	0.1	0.1	0.1	0.1	0.1	0.1	0.1	0.2	0.1	0.1	0.1	0.1	0.1	0.1	0.1	0.1	T /1/	T /1/	T /1/
C_4H_8	0.1	0.1	0.1	0.1	0.1	0.1	0.1	0.2	0.1	0.1	0.1	0.1	0.1	0.1	0.1	0.1	T /1/	T /1/	T /1/
$n\text{-}C_4H_{10}$	79.9	75.3	62.0	35.3	32.2	20.8	20.0	50.4	33.0	27.8	27.3	19.8	18.0	13.2	14.7	6.5	4.4	4.5	1.7
Steam in Product, mole frac	0.907	0.901	0.883	0.815	0.803	0.733	0.728	0.863	0.807	0.775	0.783	0.729	0.715	0.671	0.675	0.547	0.476	0.521	0.326
Methane Production, moles/ mole feedstock converted	0.138	0.0	0.0	0.053	0.0	0.165	0.137	0.0	0.0	0.0	0.0	0.142	0.415	0.327	0.227	0.491	0.630	0.707	0.551
Calculated Water Gas Shift Constant	0.195	0.143	0.278	0.851	0.710	0.990	1.16	0.128	1.09	0.193	0.456	0.346	1.09	0.471	1.09	0.928	1.90	0.526	9.20
Calculated Steam-Methane Constant	-	-	-	-	-	-	-	-	-	-	-	0.0635	0.0109	0.0506	0.0470	0.138	0.178	0.141	0.442

/1/ Trace. Less than 0.1 mole per cent.

FILE NO. E-3115
JCY:PS 11/12/59

Figure 1

EFFECT OF PARAFFIN HYDROCARBON MOLECULAR WEIGHT ON OPERABILITY

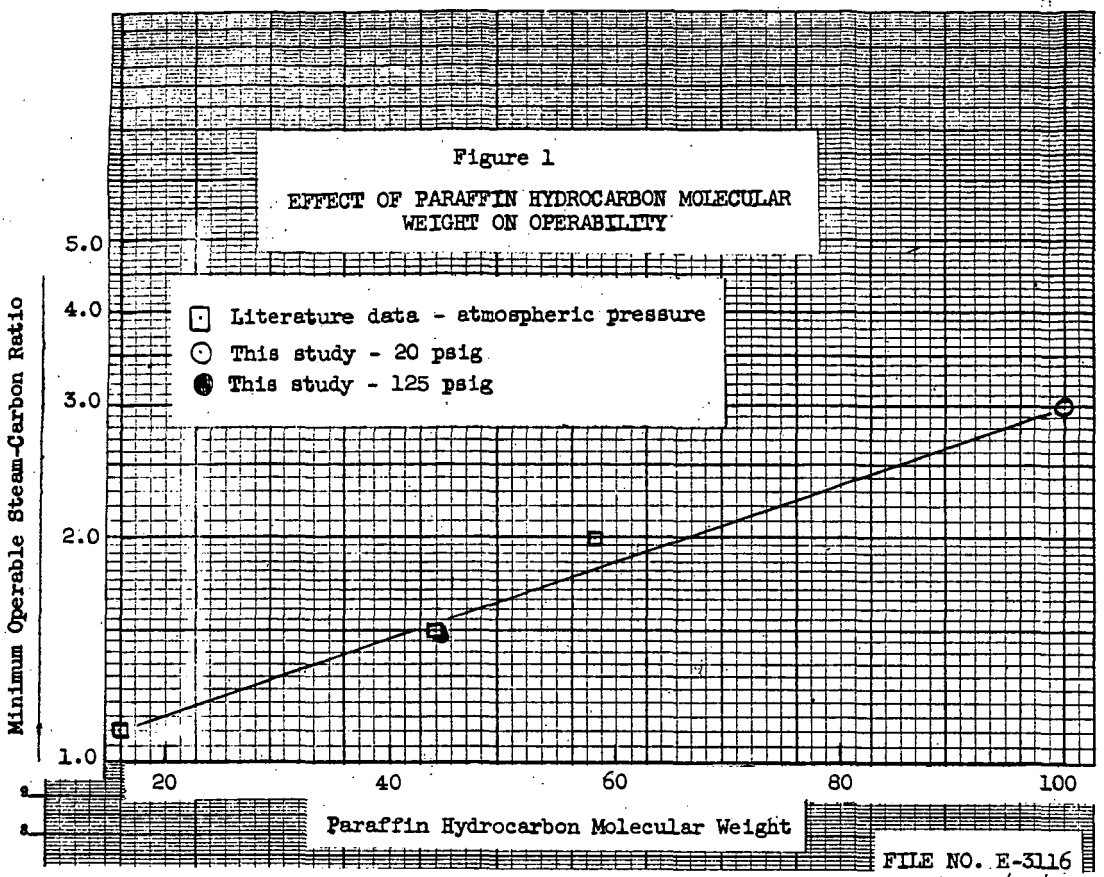

FILE NO. E-3116
JCY:LA 11/12/59

Figure 2

METHANE PRODUCTION WHEN REFORMING BUTANE TO PARTIAL CONVERSION

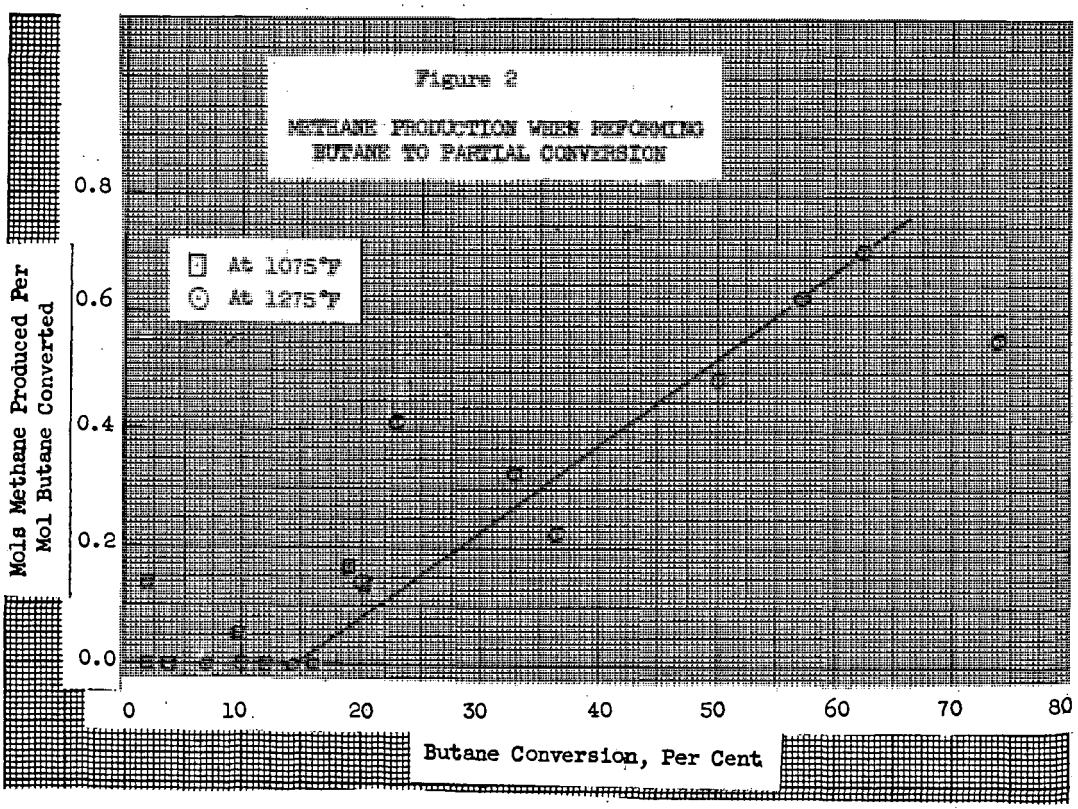

TRANSFER OF HEAT FROM HELIUM AT HIGH TEMPERATURES-- PHYSICAL CHARACTERISTICS OF CERAMIC HEAT EXCHANGERS

Stanley C. Browning* and John J. S. Sebastian

Morgantown Coal Research Center
Bureau of Mines, U. S. Department of the Interior
Morgantown, W. Va.

Preliminary cost studies indicate that it should be economically possible to use nuclear energy as process heat for certain endothermic reactions. The Federal Bureau of Mines' interest at present is utilizing heat from the fission of nuclear fuels to gasify coals with steam to produce synthesis gas. Of primary concern in the study of the use of nuclear heat for gasification of coal and for other industrial purposes is the problem of effective transfer of heat from the gas-cooled nuclear reactor-core to a reaction chamber where the endothermic reaction takes place. In order to remove the heat from the coolant-gas, it is necessary to design a heat exchanger capable of performance at temperatures much in excess of those ordinarily encountered in heat exchange equipment. Heat exchangers constructed of available metals will not withstand prolonged use at high temperatures. This suggests the investigation of certain ceramic materials capable of withstanding high temperatures and other severe conditions of corrosion and erosion.

Much data are available in the literature on heat transfer by forced convection to and from gases. Summaries of previous work have been published by McAdams (15) and others (8, 11). Most of the existing experimental data, however, refer primarily to heat exchange in metal tubes, and do not extend into the range of higher temperatures in which interest has increased in many current engineering applications.

An experimental investigation was undertaken at the Morgantown Coal Research Center of the Bureau of Mines, U. S. Department of the Interior, Morgantown, W. Va., to obtain heat-transfer information over a wide range of surface and fluid temperatures, with helium as the heat-transfer medium. As part of this broad program, an investigation was made of the transfer of heat from helium (flowing through smooth tubes) to the tubular surfaces of a vitreous alumina heat exchanger. The effects of such variables as tube-wall temperature and inlet helium temperature were investigated. The feasibility of the use of ceramic materials in a heat exchanger and some of the factors involved in the design and fabrication of a ceramic exchanger were also studied.

In most of the forms of heat-exchange apparatus based on forced convection the velocity of the fluid is maintained at a sufficiently high level to assure a turbulent flow. In this investigation, however, it was not possible to attain turbulent flow because of the low density of helium at atmospheric pressure and the increasing viscosities of gases with temperature. The pressure could not be increased above atmospheric as it was necessary to hold the helium loss from the system within practical limits. Consequently, this investigation was conducted in the lower laminar flow region at atmospheric pressure.

*Present address, Glen L. Martin Co., Baltimore, Md.

Complete mathematical solution is known for only a relatively few cases of heat transfer. Since this problem involves so many variables, a mathematical expression for the transfer of heat through the fluid film is usually developed by the method of dimensional analysis. Attempts to solve the Fourier-Poisson equation have met with little success, mainly because of the hydrodynamic problem that must be solved simultaneously. The completed solutions of the Fourier-Poisson equation depend on convenient assumptions concerning the motion of the fluid.

Drew (6) eliminates most of the proposed solutions and lists only three for the case of a jacketed tube or pipe, i.e. those of Graetz, Leveque and Russell. Several investigators (4, 7, 16) evaluated Graetz' results for the conduction of heat in fluids moving in laminar flow. Other equations (5, 13, 14, 18) derived for the calculation of the Nusselt number from the velocity distribution vary in form due to the various assumptions used in deriving them.

For laminar flow, McAdams (15, 19) recommends an empirical expression for calculating the inside-film heat-transfer coefficient:

$$\left(\frac{h}{CV\rho}\right)\left(\frac{C\mu}{k}\right)^{2/3}\left(\frac{\mu_w}{\mu}\right)^{0.14} = 1.86\left(\frac{D}{L}\right)^{1/3}\left(\frac{DV\rho}{\mu}\right)^{-2/3} \qquad (1)$$

This relationship applies for Reynolds numbers below 2100, but it would give incorrect heat-transfer coefficients for very low "Re" numbers.

Theoretical formulas, such as those of Graetz, for heat transfer to fluids in viscous flow in tubes, do not take into consideration the effects of the radial temperature gradient on the axial and radial components of velocity. Because of the temperature coefficient of viscosity, a radial viscosity gradient results that affects the distribution of velocities considerably compared to that prevailing in isothermal flow. This presents a problem of deciding where, and at what temperature, the physical properties of the fluid should be evaluated. Colburn (4) obtained good correlation of data on heat transfer by employing film properties, but had to supplement his correlation by introducing a viscosity correction ratio.

Sieder and Tate (19) simplified calculations by basing their correlations on main stream properties. To express the interaction of the viscosity gradient on the velocity distribution, they included in the usual correlation of dimensionless numbers an additional dimensionless group, μ_a/μ_w, i.e., the ratio of the viscosity at the average helium temperature to that at the wall temperature.

The correlations heretofore discussed were made at relatively low temperatures; only limited data exists for heat transfer at higher temperatures. Zellnik and Churchill (20) obtained data for the transfer of heat from air in turbulent flow inside a tube for temperatures of 480 - 2000°F. and flow rates corresponding to Reynolds numbers from 4500 to 22,500. Others (10) have published some data on heating air inside a tube with wall temperatures up to 2950°F. More recently, Ramey, Henderson and Smith (17) determined heat-transfer coefficients for air flowing in a 2-inch pipe at temperatures of 500 - 1200°F., with gas-to-wall temperature differences of 300 to 1000°F., and Reynolds numbers from 2000 to 20,000. Their results include data on steam over a range of Reynolds numbers from 5000 to 60,000.

However, all these high-temperature heat-transfer studies pertain to turbulent flow. The data pertaining to turbulent flow at high temperatures deviated from those relating to low-temperatures when correlated by the proposed theoretical equations.

Apparatus and Procedure

A schematic diagram of the apparatus used for our study of heat transfer at high temperatures, is shown in Figure 1. Helium was recycled in a closed circuit by

means of a rotary positive-displacement blower. The helium from the pump was passed through a surge tank and heated to the desired temperature in a resistance-type electric furnace. This temperature was measured by a shielded thermocouple placed in a mixing chamber located between the outlet of the furnace and the inlet to the "test-section", i.e., that part of the train in which the tested heat exchanger is inserted. The helium temperature was measured also at the outlet from the test-section before entering the cooler. The helium cooled to room temperature was passed through two parallel-connected calibrated rotameters to measure the rate of flow of the heat transfer medium through the closed circuit. The test-section, shielded thermocouples, and adjoining tubing were thermally insulated. Additional helium to replace that which leaked from the system was supplied through a pressure-regulator. The flow rate of this "make-up" gas was indicated by a calibrated rotameter.

Compressed air was supplied as heat receiving medium to the annulus of the test-exchanger. The wall temperature of the inner tube of the test-exchanger was regulated by changing the rate of flow of the air through the annular space. High tube-wall temperatures were obtained by preheating this air in a commercial electric resistance furnace. The direction of flow of gases in the exchanger could be altered from concurrent to countercurrent, or vice-versa, simply by switching the inlet and outlet valves for the air or any other cooling fluid used as heat absorbers. The temperature of the cooling air was measured at the inlet and outlet of the heat exchanger; its flow-rate was measured by a calibrated rotameter.

A test-exchanger made of vitreous alumina, with a length-to-diameter ratio of 60, was used (Figure 2). The vitreous alumina inner tubing was surrounded by a larger diameter tube of the same material, and the cooling air was passed through the annular jacket thus formed. Tube wall temperatures were measured by means of (Pt)-(Pt+10 percent Rh) thermocouples located at ten different points along the tube length. Each thermocouple was placed in a slot cut halfway through the tube wall and covered over with alumina cement. The thermocouples were connected by means of a selector switch to a potentiometer.

The physical properties of the helium were computed by extrapolation of available published data. The thermal conductivity and viscosity data were taken from the results of work done at the National Bureau of Standards by Hilsenrath and Touloukian (9). The specific heat of helium at constant pressure (1) was taken as 1.24 B.t.u./(lb)(°F.). This value agreed with that calculated from the Prandtl numbers and viscosity and thermal conductivity data of Hilsenrath and Touloukian and was assumed constant, since the specific heat of helium does not vary with temperature.

Experimental Results and their Evaluation

The average temperature of the helium ("hot gas"), T_a, was taken as the average of the inlet, T_i, and outlet, T_o, temperatures. Each of these temperatures was measured by a "shielded thermocouple" arrangement through which the hot helium had passed and was thoroughly mixed.

Average inside tube-wall temperatures were determined for various flow rates of helium and cooling air; typical results are illustrated for counterflow of gases in Figure 3, and for parallel flow in Figure 4. The rate of heat transfer (Q), the helium flow rate (V), average wall temperature (t_w), and the helium temperature at the inlet (T_i) are shown as parameters. The curves obtained are typical temperature distribution curves; similar trends were obtained for other conditions of flow and gas temperatures.

The average wall temperatures of the inner tube of the test-exchanger were obtained by measuring the area under curves similar to those in Figures 3 and 4 and dividing it by the length of the heat-transfer area. Thermocouples embedded in the tube wall were assumed to measure the temperature of the inside surface of

the tube. The fact that the calculated temperature gradients through the wall were found to be negligible, less than 3°F., justifies the assumption. The average inside-film heat-transfer coefficient (h_i) was obtained from the experimental data by the relation:

$$h_i = \frac{WC\ (T_i - T_o)}{A\ (t_w - T_a)} \tag{2}$$

As pointed out previously, the usual method of correlating experimental data on heat transfer by forced convection is being employed by determining the effects of significant variables on the rate of heat transfer and combining these variables into an empirical equation by means of dimensional analysis. The equation obtained by this method is:

$$\frac{h_i D}{k} = K \left(\frac{DV\rho}{\mu}\right)^m \left(\frac{C\mu}{k}\right)^n \left(\frac{L}{D}\right)^p \tag{3}$$

where K is a constant and m, n and p are exponential constants. McAdams (15) suggested a simpler form of this equation, derived by assuming that m, n and p are equal:

$$\frac{h_i D}{k} = K \left(\frac{4}{\pi} \frac{WC}{kL}\right)^a \tag{4}$$

The experimental data obtained in this investigation were correlated by use of both types of equations. However, Equation (3) gave a better representation of the data from our ceramic heat exchanger for the L/D ratios employed. To establish a more general equation valid for any L/D ratio, additional investigation is necessary to cover a wider range of experimental conditions.

The experimental data obtained were first correlated in terms of Equation (4). For this purpose, the viscosity and thermal conductivity data used had been computed for the average gas temperature.

Data obtained by use of helium cooled by air in a vitreous-alumina heat exchanger, having a length-diameter ratio of 60, are presented in Figure 5. The data shown refer to inlet-gas temperatures of 1450 - 2665°F. and Graetz numbers of 0.03 - 5. A group of three parallel straight lines, each for a different condition of cooling-air flow, has been obtained. The plot shows conclusively that either by reducing the velocity of the cooling air or by heating it, the trend -lines shifted in position, and a different value was obtained for the constant, K. That is to say, there is a difference in Nusselt number for any selected value of Graetz number. Since varying the velocity or increasing the inlet temperature of cooling air had the effect of varying the tube-wall temperature, it seemed obvious that a satisfactory correlation would require inclusion of the surface temperature, or of properties that are dependent upon the latter.

When the average temperature is used for the evaluation of heat transfer properties, no allowance is being made for the variation of these properties over the cross section of the flowing fluid. However, these variations influence the heat exchange within the fluid. The Seider and Tate viscosity correction takes into account variations of viscosity, but ignores the other properties. The use of a gas-to-wall temperature ratio, on the other hand, corrects for variations in the velocity profile with temperature. But, as these velocity variations are caused by changing physical properties due to temperature changes, the T_a/t_w ratio actually corrects for all changes in the physical properties with temperature. Therefore, application of the temperature-ratio corrections would be expected to result in a better correlation. Consequently, the $\frac{4}{\pi}\frac{WC}{kL}$ group was supplemented by

addition of the T_a/t_w ratio. The final form of Equation (4) thus became:

$$\frac{h_i D}{K} = K \left(\frac{4}{\pi} \frac{WC}{kL}\right)^a \left(\frac{T_a}{t_w}\right)^b \qquad (5)$$

where: $h_i D/k$ is the Nusselt number (Nu), and WC/kL is the Graetz number (Gz).

Several runs were made holding the Graetz number constant in order to determine the extent of the dependence of Nusselt number on the temperature ratio. The results of these tests are shown in Figure 6. The average value of the exponent b, obtained by taking the slope of these curves, was found to be -0.9 for values of T_a/t_w less than approximately 3. It can be seen from Figure 6 that any further increase in the gas-to-surface temperature ratio above 3 has practically no effect on the Nusselt number.

In laminar flow, when a fluid flows isothermally the velocity profile is assumed to be parabolic, with a maximum velocity at the center axis of the pipe or tube, and zero velocity at the wall. The flow may be thought of as concentric cylindrical elements of fluid moving relative to each other with little or no mixing of the layers. If the hot stream of gas is being cooled, as in this investigation, the viscosity of the gas near the wall is lower than that of the main stream of the fluid; consequently, the fluid near the wall travels at a higher velocity than normally when the wall is not cooled. For this to happen, some of the gas from the center of the tube must flow toward the wall to maintain the increased velocity at the tube-wall. Thus, the cooling of the fluid causes a radial component of velocity that modifies the nature of the laminar flow.

Since in cooling the gas the parabolic distribution of velocity is distorted, correction should be applied. As the difference in gas and wall temperatures increases, T_a/t_w increases, it is expected that the velocity profile would tend to approximate that of a well-mixed fluid, and the properties would not vary appreciably across a section of the tube. Further increase in T_a/t_w would not be expected to change the velocity profile appreciably; the properties of the fluid would remain essentially the same across the tube section and no correction would be needed.

For values of T_a/t_w less than 3, Equation (5) can be written as:

$$\frac{h_i D}{k} = K \left(\frac{4}{\pi} \frac{WC}{kL}\right)^a \left(\frac{T_a}{t_w}\right)^{-0.9} \qquad (6)$$

This equation was rearranged into a more useful form for plotting:

$$\log \left[\frac{h_i D}{k} \left(\frac{T_a}{t_w}\right)^{0.9}\right] = a \log \left(\frac{4}{\pi} \frac{WC}{kL}\right) + \log K \qquad (7)$$

The value of constant "a" was found to be 0.86 from a plot of this equation, Figure 7, by measuring the slope of the trend-curve (a straight line) obtained by the best free fit. From the same plot, for the value of "K" 1.10 was obtained as the intercept on the ordinate at unity on the abscissa. The plotted data have been corrected for differences between the gas and wall temperatures.

Substituting the values of K, a and b into Equation (5), the following equation:

$$\frac{h_i D}{k} = 1.10 \left(\frac{4}{\pi} \frac{WC}{kL}\right)^{0.86} \left(\frac{T_a}{t_w}\right)^{-0.9} \qquad (8)$$

was obtained for values of T_a/t_w less than 3.

For values of T_a/t_w greater than 3, a plot of the experimental data based on Equation (4) gave a similar straight line (Figure 8). No correction has been applied in this plot for differences between the gas and wall temperatures for the reasons already discussed.

A better correlation of the experimental data was obtained by Equation (3) which contains the dimensionless groups associated with turbulent flow:

$$\frac{h_i D}{k} = K \left(\frac{DV\rho}{\mu}\right)^m \left(\frac{C\mu}{k}\right)^n \left(\frac{L}{D}\right)^p \qquad (3)$$

where $h_i D/k$ is the Nusselt number (Nu), $DV\rho/\mu$ is the Reynolds number (Re), and $C\mu/k$ is the Prandtl number (Pr). However, the number of length-diameter ratios (L/D) investigated was insufficient to determine their effect on the Nusselt number; therefore, the correlations presented here are applicable only to the values of L/D investigated.

In Figure 9 the heat-transfer coefficients are correlated with other pertinent variables in terms of the Reynolds (Re), Prandtl (Pr), and Nusselt (Nu) numbers. Namely, the ratio of the Nusselt number to the cube root of the Prandtl number ($Nu\ Pr^{-1/3}$) was plotted against the Reynolds number (Re). Two parallel straight lines, one for a lower and one for a higher flow-rate of cooling-air, have been obtained. For computing the numerical values of these dimensionless groups for plotting, the values of viscosity, thermal conductivity, specific heat and other physical properties of the helium have been estimated at the average stream temperatures.

If corrections are incorporated for differences in helium-stream and wall temperatures, the curve in Figure 10 is obtained for values of T_a/t_w less than 3. The slope of this trend line is 0.86 and the intercept on the ordinate at Re = 1 is 0.028. Thus, Figure 10 represents a plot of the following equation:

$$\frac{h_i D}{k} \left(\frac{T_a}{t_w}\right)^{0.9} \left(\frac{C\mu}{k}\right)^{-1/3} = 0.028 \left(\frac{DV\rho}{\mu}\right)^{0.86} \qquad (9)$$

Transposing, Equation (10) is obtained, which adequately represents the experimental data:

$$\frac{h_i D}{k} = 0.028 \left(\frac{DV\rho}{\mu}\right)^{0.86} \left(\frac{C\mu}{k}\right)^{1/3} \left(\frac{T_a}{t_w}\right)^{-0.9} \qquad (10)$$

for values of T_a/t_w less than 3.

The heat-transfer data obtained in this work is of limited scope due to the low helium flow-rates used. The heat-transfer curves should not be extrapolated beyond the range of values plotted, as a change in the slope of the curve for Graetz numbers above 5 has been indicated in our investigations.

The gas-to-wall temperature ratio was used as a correction factor instead of the viscosity ratio correction of Sieder and Tate (19). Consequently, the gas-wall temperature correction would not be applicable to a gas whose physical properties are affected by temperature differently than those of helium. Likewise, the point at which the temperature ratio ceases to influence the heat-transfer curve would be expected to be different for other gases.

Free convection effects were neglected in this investigation since the tubes used were horizontal and were of relatively small diameters. In larger tubes, free convection would be expected to influence the heat transfer as long as laminar flow was maintained.

In view of the low flow-rates, it was assumed that end effects were negligible and that laminar flow was maintained within the test section.

Problems in the Design of Ceramic Heat Exchangers

The difficulties encountered in the design and construction of our experimental vitreous alumina exchanger indicate that several construction problems remain to be solved before a ceramic heat exchanger could be produced commercially. The greatest of these problems is that of making and maintaining several gastight seals, some of which must withstand temperatures exceeding 2500°F.

These seals must be made with some type of cementing material, which when dried and fired will have a coefficient of expansion similar to that of the materials joined. As much of the piping and auxiliary apparatus used with the exchanger is metallic, it is necessary to join materials with greatly different coefficients of expansion. No satisfactory solution to this problem has yet been found.

In our experimental work the most effective joints, both ceramic-to-ceramic and ceramic-to-metal, were obtained by using a mixture of 60-70% fine grain (ball-milled for 16 hours) pure alumina plus 30-40% commercial sodium silicate solution. After the cement had air-dried, the joints were fired at temperatures above 2200°F. Several successive coatings of this cement were applied, and the drying-firing process was repeated. However, joints of this type have not always been satisfactory.

After approximately 1000 hours of operation, our experimental alumina heat exchanger was removed from the test circuit to test the seals for gas leaks. While some of the joints were found to be gastight at low pressures (5 p.s.i.g.) others were not. Also, after an extended period of operation at high temperatures, the alumina cement had a tendency to peel off the metal in case of metal-to-ceramic joints.

The difficulty of constructing effective ceramic seals was also realized under actual operating conditions. In all tests enough helium was supplied to the cycling system to maintain a slightly positive pressure in the test loop. With higher pressure drops, caused by attempts to increase the helium flow rates in the system, it became necessary to increase the helium makeup to maintain the pressure. The makeup rate (helium loss) eventually became so great that it was no longer practical to continue to increase the gas cycling rate. Thus, pressure drops above 16-inch w.g. could not be tolerated. At very low flow-rates, on the other hand, experiments have been continued for several days without adding any helium as makeup.

In addition, definite precautions had to be taken to prevent failure of the tubes from thermal shocks. Although, vitreous alumina has remarkably high resistance to thermal shocks compared to most ceramic materials, elaborate precautions had to be taken to avoid fracture from thermal stresses. Care was taken during heating and cooling periods to avoid large thermal gradients likely to cause tube failure.

Efforts have been made recently by several investigators (1) to predict the ability of basic components of ceramic materials to withstand thermal stresses encountered in service. Of particular interest in the investigations of Baroody and associates (2) was the high resistance to thermal fracture exhibited by thin-walled tubes such as might be used in ceramic heat exchangers.

Another problem in the design of ceramic exchangers is that of expansion. Any type of expansion joint adds to the task of maintaining a leak-proof cycling system. When providing for expansion, it should be desirable to keep the components of the exchanger in a state of compression rather than tension, as ceramics are relatively weak in tension. No special precautions were necessary for the expansion of the exchanger parts in this investigation since the outer tube was large compared to the inner tube, and the stresses encountered were considered safely below the limit.

Conclusions

Correlations for the prediction of the average inside-film coefficients of heat-transfer for the removal of heat from gases in the lower region of laminar flow, with high temperature differences prevailing, must include a correction for the variation of fluid properties up to a certain value of gas-to-wall temperature ratio. Beyond this point, any increase in this temperature ratio ceases to influence the heat transfer relationship.

Within the limits of this investigation, and for gas-to-surface temperature ratios less than 3, the experimental data for helium may be represented by the equation:

$$Nu = 0.028\ (Re)^{0.86}\ (Pr)^{1/3}\left(\frac{T_a}{T_w}\right)^{-0.9}$$

or:

$$Nu = 1.10\left(\frac{4}{\pi}Gz\right)^{0.86}\left(\frac{T_a}{t_w}\right)^{-0.9}$$

Ceramic heat exchangers appear to hold much promise for use in temperature ranges above those generally encountered in conventional exchangers. However, no progress is in sight in their design and construction until methods are developed to construct mechanically reliable gastight seals, and means are found to prevent high thermal stresses. Both of these problems would arise in a commercial size heat exchanger of this type under operating conditions. Ceramic heat exchangers are also limited at present to low pressures that makes their use with a light, gaseous heat-transfer medium, such as helium, impractical.

Acknowledgment

The work described was carried out as part of the A.E.C. - Bureau of Mines process-heat reactor program for the utilization of nuclear energy for coal gasification. The authors are indebted to the Atomic Energy Commission for partial support of the research conducted.

Thanks are due L. L. Hirst and R. F. Stewart for helpful suggestions made at various times during the course of the work, and to H. G. Lucas for assistance in the experimental work.

Nomenclature

A = heat transfer surface, ft.^{2}
C = specific heat at constant pressure, B.t.u./(lb.)(°F.)
D = inside diameter of tube or pipe, ft.
h = film heat-transfer coefficient, B.t.u./(hr.)(ft.^{2})(°F.)
k = thermal conductivity, B.t.u./(hr.)(ft.^{2}) (°F./ft.)
L = length, ft.
Q = heat flow, B.t.u./hr.
R = resistance to heat flow, (hr.)(ft.^{2})(°F.)/B.t.u.
T_i = temperature of helium at inlet, °F.
T_o = temperature of helium at outlet, °F.
T_a = average helium temperature, °F.
t_i = temperature of cooling gas at inlet, °F.
t_o = temperature of cooling gas at outlet, °F.
t_1, t_2, t_3 = wall temperatures at selected points along the tube length, °F.
t_w = average wall temperature, °F.
V = velocity, ft./hr.; or total volume, ft.^{3}
v = specific volume, ft.^{3}/lb.
W = weight flow rate of helium, lb./hr.
μ = viscosity, lb./(ft.)(hr.)
ρ = density, lb./ft.^{3}
x = distance, ft.
a, m, n, p, b = constants

Dimensionless Numbers

WC/kL = Graetz number (Gz)
hD/k = Nusselt number (Nu)
$C\mu/k$ = Prandtl number (Pr)
DG/μ = Reynolds number (Re)

Subscripts

i = inside of pipe or tube
o = outside of pipe or tube
f = film
a = hot gas
w = wall
m = mean value

Literature Cited

(1) Baroody, E. M., Duckworth, W. H., Simons, E. M., Schofield, H. Z.,"Effect of Shape and Material on the Thermal Rupture of Ceramics", U. S. Atomic Energy Comm., Nat'l Sci. Foundation, AECD - 3486, 5-57 (1951).
(2) Baroody, E. M., Simons, E. M., Duckworth, W. H., "Effect of Shape on Thermal Fracture", J. Am. Ceramic Soc., 38, (1955).
(3) Browning, S. C., Masters Thesis, West Virginia University, Morgantown, W. Va., 1959.
(4) Colburn, A. P., "Method of Correlating Forced Convection Heat Transfer Data and a Comparison with Fluid Friction", AIChE Trans., 29, 174 (1933).
(5) Deissler, R. G., "Investigation of Turbulent Flow and Heat Transfer in Smooth Tubes Including the Effects of Variable Properties", ASME Trans., 73, 101 (1951).
(6) Drew, T. B., "Mathematical Attacks on Forced Convection Problems: A Review", AIChE Trans., 26, 26 (1931).
(7) Drew, T. B., Hogan, J. J., McAdams, W. H., "Heat Transfer in Streamline Flow", Trans. AIChE, 26, 32 (1931).
(8) Groeber, H., Erk, S., Grigull, U., Die Grundgesetz der Warmeubertragung, Springer Verlag, Berlin, Germany, 3rd ed., 1955.
(9) Hilsenrath, J., Touloukian, Y. S., "The Viscosity, Thermal Conductivity and Prandtl Number for Air, O_2, N_2, NO, H_2, CO, CO_2, H_2O and A", ASME Trans., 79, 967-985 (1954).
(10) Humble, L. V., Lowdermilk, W. H., Desmond, L. G., "Measurements of Average Heat-Transfer and Friction Coefficients for Subsonic Flow of Air in Smooth Tubes at High Surface and Fluid Temperatures", NACA Report 1020, (1951).
(11) Knudsen, J. G., Katz, D. L., "Fluid Mechanics and Heat Transfer", McGraw-Hill, New York, 1958.
(12) Lee, J. F., Sears, F. W., "Thermodynamics", Addison Wesley, Reading, Mass., 1956.
(13) Lyon, R. N., "Heat Transfer at High Fluxes in Confined Spaces", Chem. Engr. Progr. 47, 75 (1951).
(14) Martinelli, R. C., "Heat Transfer to Molten Metals", ASME Trans., 69, 947 (1947).
(15) McAdams, W. H., "Heat Transmission", McGraw-Hill, New York, 1942.
(16) Norris, R. H., Streid, D. D., "Laminar-Flow Heat-Transfer Coefficients for Ducts", ASME Trans., 62, 525 (1940).
(17) Ramey, H. J., Henderson, J. B., Smith, J. M., "Heat-Transfer Coefficients for Gases; Effect of Temperature Level and Radiation", Chem. Eng. Progr. 50, Sym. Ser. No. 9, 21-28, (1954).
(18) Seban, R. A., Shimazaki, T. T., "Heat Transfer to a Fluid in a Smooth Pipe with Walls at a Constant Temperature", ASME Trans., 73, 803 (1951).
(19) Sieder, E. N., Tate, C. E., "Heat Transfer and Pressure Drop of Liquids in Tubes", Ind. Eng. Chem., 28, 1429 (1936).
(20) Zellnik, H. E., Churchill, S. W., "Convective Heat Transfer from High-Temperature Air Inside a Tube", Paper presented at ASME-AIChE Joint Heat Transfer Conference, (Aug. 1957).

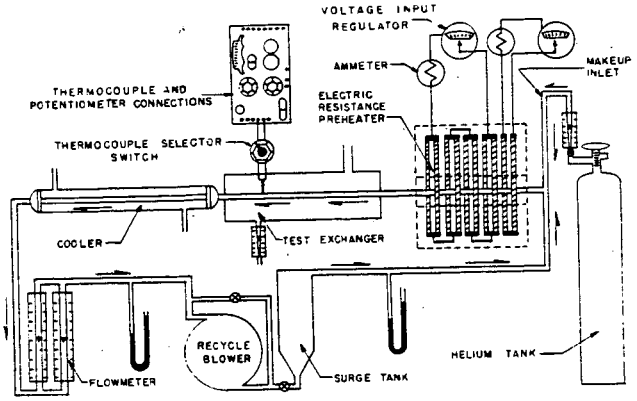

Figure 1. Flow diagram of apparatus for the study of heat transfer at high temperatures

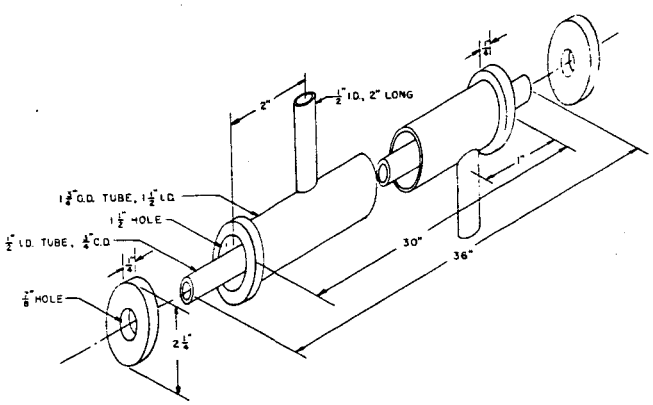

Figure 2. Construction details of vitreous alumina heat exchanger

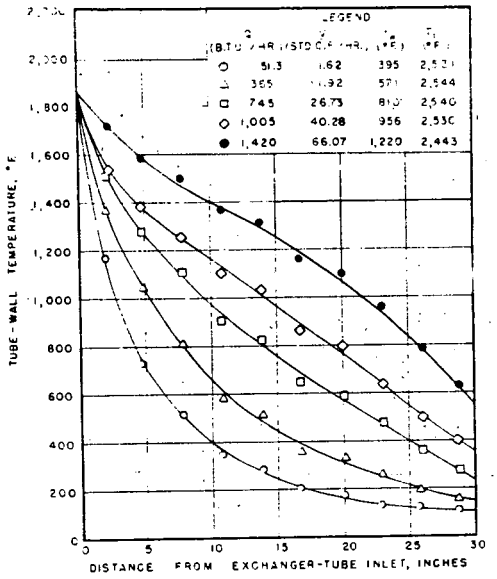

Figure 3. Distribution of tube-wall temperatures, counter flow

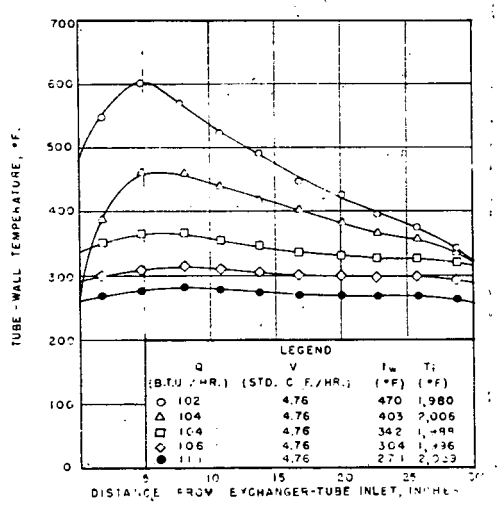

Figure 4. Distribution of tube-wall temperatures, parallel flow.

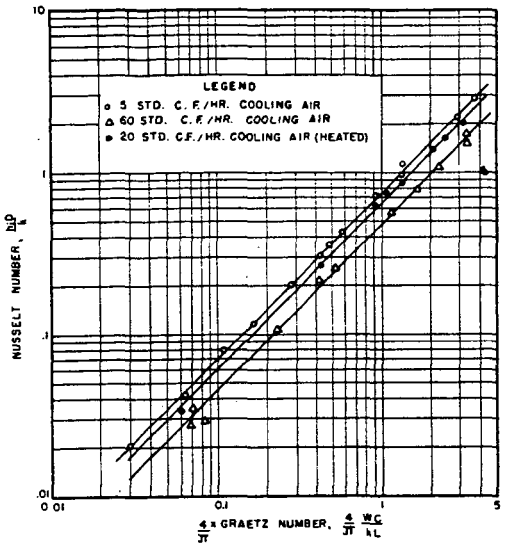

Figure 5. Correlation of heat-transfer data showing effect of cooling-air rate

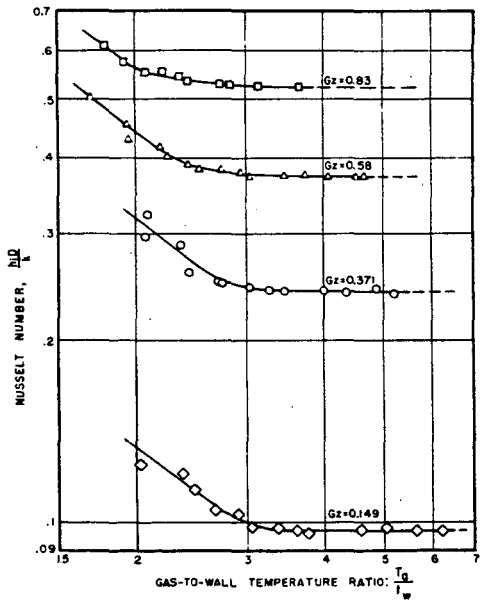

Figure 6. Effect of gas-to-wall temperature ratios on Nusselt number

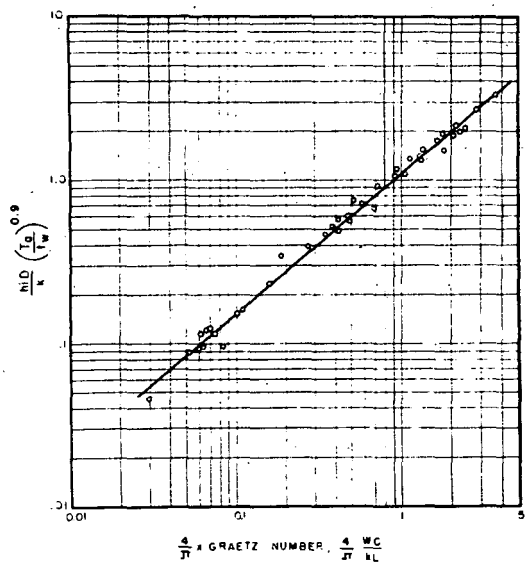

Figure 7. Correlation of heat-transfer data corrected for temperature ratios less than 3

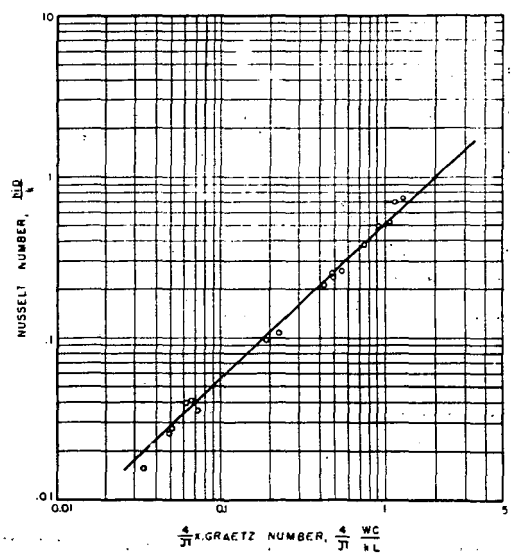

Figure 8. Correlation of heat-transfer data for temperature ratios greater than 3

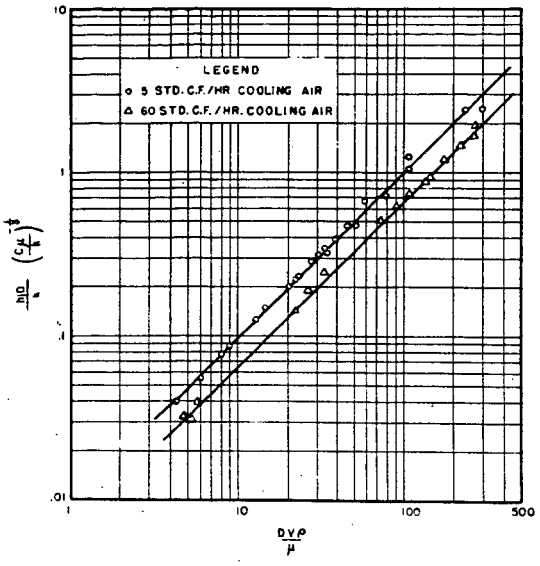

Figure 9. Correlation of heat-transfer data in terms of Reynolds number

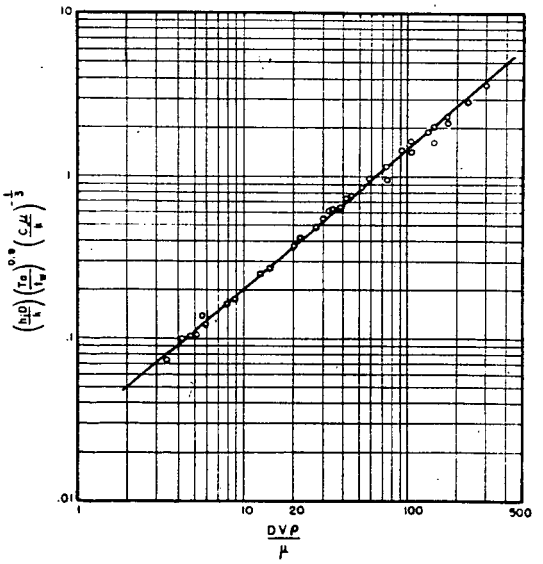

Figure 10. Correlation of heat-transfer data, corrected for temperature ratios, in terms of Reynolds number